RSC Advances

REVIEW

View Article Online
View Journal | View Issue

Cite this: *RSC Adv.*, 2022, **12**, 19590

Advances and emerging challenges in MXenes and their nanocomposites for biosensing applications

Zaheer Ud Din Babar, [ab] Bartolomeo Della Ventura, [b] Raffaele Velotta [b] and Vincenzo Iannotti *[bc]

Two-dimensional materials have unique properties and their better functionality has created new paradigms in the field of sensing. Over the past decade, a new family of 2D materials known as MXenes has emerged as a promising material for numerous applications, including biosensing. Their metallic conductivity, rich surface chemistry, hydrophilicity, good biocompatibility, and high anchoring capacity for biomaterials make them an attractive candidate to detect a variety of analytes. Despite such notable properties, there are certain limitations associated with them. This review aims to present a detailed survey of MXene's synthesis; in particular, their superiority in the field of biosensing as compared to other 2D materials is addressed. Their low oxidative stability is still an open challenge, and recent investigations on MXene's oxidation are summarized. The hexagonal stacking network of MXenes acts as a distinctive matrix to load nanoparticles, and the embedded nanoparticles can bind an excess number of biomolecules (*e.g.*, antibodies) thereby improving biosensor performance. We will also discuss the synthesis and corresponding performance of MXenes nanocomposites with noble metal nanoparticles and magnetic nanoparticles. Furthermore, Nb and Ti_2C-based MXenes, and Ti_3C_2-MXene sandwich immunoassays are also reviewed in view of their importance. Different aspects and challenges associated with MXenes (from their synthesis to final applications) and the future perspectives described give new directions to fabricate novel biosensors.

Received 11th May 2022
Accepted 21st June 2022

DOI: 10.1039/d2ra02985e

rsc.li/rsc-advances

[a]*Scuola Superiore Meridionale (SSM), University of Naples Federico II, Largo S. Marcellino, 10, 80138, Italy*

[b]*Department of Physics "E. Pancini", University of Naples Federico II, Via Cintia 26, 80126, Naples, Italy. E-mail: viannotti@unina.it*

[c]*CNR-SPIN (Institute for Superconductors, Oxides and Other Innovative Materials and Devices), Piazzale V. Tecchio 80, 80125, Naples, Italy*

Zaheer Ud Din Babar obtained his MS in Physics from National University of Sciences and Technology (NUST), Pakistan in 2019. During his master's research, he investigated the magnetic properties of Nb_2C MXene and revealed its superconductivity. Currently, he is a PhD student at the Scuola Superiore Meridionale (SSM) of the University of Naples Federico II and pursuing his project at the Department of Physics "E. Pancini". His current research interests include the synthesis of MXenes and their composites with gold and magnetic gold nanoparticles for biosensing applications.

Bartolomeo Della Ventura is a biotechnologist and assistant professor at the Physics Department "E. Pancini" of the University of Naples Federico II, Italy. He introduced a new surface functionalization procedure based on UV activation of the IgGs (Photochemical Immobilization Technique, PIT), which he is applying to several biosensors (piezoelectric, colorimetric, and electrochemical) for applications to medical diagnostics, food safety and environmental monitoring.

Introduction

Biosensing has emerged as an important area of research in recent years and currently one of the main focuses in the field of sensors. Biosensors are good alternatives to time-consuming and expensive laboratory analysis due to their ease of use, point-of-care monitoring, and rapid on-site detection. The need for efficient and sensitive biosensors with low detection limits has introduced the use of low-dimensional materials to fabricate effective transducers and efficient carriers of biorecognition elements for the sensing assembly. Over the past few decades, 2D materials have attracted increasing attention due to their dimensionality and versatile properties. Large surface/volume ratio, catalyzing behavior, and outstanding optical properties of various 2D materials *e.g.*, atomically thin graphene, transition metal dichalcogenides (*e.g.*, MoS_2, WS_2), and black phosphorus have improved the analytical performance of biosensors.[1–6] For instance, graphene offers greater electrocatalytic capacity, and MoS_2 optical biosensors are considered better than their electrochemical counterparts. These established 2D systems exhibit unique properties and produce interesting physics, however, they have some limitations, such as cytotoxicity and easy aggregation in a physiological environment.[7–10] The lack of intrinsic surface terminations in these materials leads to ineffective immobilization of bioreceptors on the electrode surface, thus increasing the assays time and decreasing the sensitivity. Moreover, the hydrophobicity of these materials results in compromised stability, and low electrical conductivity limits the signal transduction of the sensing device. So, in pursuit of novel biosensing nanoplatforms, it is essential to examine new materials with good biocompatibility, intrinsic anchoring sites, and better dispersion capability. MXenes, a family of 2D materials with layered structures of early transition metal carbides and/or nitrides have attracted huge attention since their first report in 2011.[11] MXenes possess exceptional properties and have been widely used in many applications such as energy storage,[12–14] electromagnetic interference shielding,[15] biomedical engineering,[16] electrocatalysis,[17] gas detection,[18] photocatalysis and water splitting,[12,19] magnetism,[20–22] superconductivity,[23–25] magnetotransport,[26,27] and many more.[28] MXenes hold an excellent photothermal conversion capability and have been employed in various applications such as solar photothermal electrodes, solar water desalination, and numerous biomedical applications including drug delivery, photothermal therapy, and photoacoustic imaging.[29] Since its early reports on biosensing, it has aroused a tremendous interest in the biosensing community and the past 5 years can be regarded as a gold rush in MXene biosensing. Metallic conductivity ($\approx$20 000 S cm^{-1}),[30] rich surface chemistry,[31] negligible cytotoxicity,[32] inherent hydrophilicity,[33] ability to form stable colloidal suspensions[34] and unique optoelectronic properties[35] render MXenes a promising material in biosensing. MXenes also provide an effective interface for biofunctionalization with numerous anchoring sites and enhanced electron transfer makes it a highly efficient signal transducer, hence enhancing the detection sensitivity. The rapid development of wearable electronics and the development of flexible sensors for next-generation applications (from clinical diagnostics to personalized human monitoring) has transformed the current trends in biosensing.[36] In this respect, conducting polymers (CPs) can be effective due to several promising features such as high mechanical strength, easy synthesis, and high environmental stability. Moreover, CPs offer facile immobilization of enzymes and effectively facilitate the charge transfer to develop various biosensors and designing biofuel cells.[37] There are however some limitations associated with CPs in their pristine forms such as high detection limits, slow response time, cytotoxic nature, and differences in *in vitro* and *in vivo* studies.[38] To overcome these limitations, various strategies to fabricate composite of CPs with nanomaterials have been introduced.[39] It is well-known that MXenes do not require chemical or thermal reduction treatment which makes their integration into CPs easier as compared to graphene coupled conducting polymers.[40] MXene imparts new

Raffaele Velotta is presently professor of physics at the University of Naples Federico II where he obtained his PhD in 1992. For several years, his research concerned laser physics, nonlinear optics, and ultrashort pulse generation. In the last ten years, he devoted himself to biosensing with particular focus to the realization of immunosensors (piezoelectric, electrochemical and optical) for detecting toxic molecules, proteins and bacteria. His current interests include immunosensors based on nanostructured surface (plasmon enhanced fluorescence) and magnetic nanoparticles.

Vincenzo Iannotti is currently associate professor at the Department of Physics "E. Pancini" of the University of Naples Federico II where he obtained his PhD in 1999. His research interests focused on nanostructured magnetic materials and their composites for sensing applications. He is currently investigating the application of magnetic nanoparticles and 2D materials (MXenes) in biosensing.

functionalities, for example, intrinsic terminations on the surface of MXenes allow them to adhere to the CPs quite effectively thus improving the signal conduction. Functional groups participate actively in the fabrication of highly effective strain sensors, allowing crack propagation and dominating the sensing phenomenon by drastically reducing electrical resistance under applied stress. Henceforth, MXenes are promising candidates to overcome the limitations associated with materials already well-known for their use in biosensing and to realize state-of-the-art biosensing platforms, both electrochemical and optical, and have thus been able to satisfy the present quest for a new 2D material for biosensing applications. Several reviews on MXene-based electrochemical biosensors,[41–43] optical biosensors,[44] and biofuel cell designs[45] have recently been published with particular attention on Ti_3C_2 MXene. In this paper, we aim at providing insights on the applications of MXenes – as well as their nanocomposites – as signal transducers and efficient carriers of biomolecules. Thus, special emphasis is placed on the material aspects, fundamental properties, and associated challenges with using MXenes and their nanocomposites in biosensors. With a comprehensive review on the chemical stability of MXenes and integration of nanoparticles, we will see how Ti_3C_2 MXene and its composites with noble metal nanoparticles are used as signal transducers as well as amplification tags in various sandwich immunoassays for sensitive detection of various analytes. Further, in view of their potential in sensing, we have addressed the properties and applications of Ti_2C, Nb_2C, and Nb_4C_3 MXenes in various electrochemical and optical biosensing platforms.

Survey on MXenes synthesis

MXenes, a new class of 2D materials has attained a huge interest due to certain unique properties over existing 2D materials. MXenes are layered structures of carbides and nitrides of early transition metals derived from 3D MAX phases. Layered MAX phases with general expression $M_{n+1}AX_n$ have a hexagonal structure with $P6_3/mmc$ space group symmetry and they represent unusual ceramic and metallic properties.[46] Till now, there are more than 70 MAX phases are reported.[14] Added to this, almost 40 MXenes are obtained experimentally *e.g.*, $Ti_3C_2T_x$, Ti_2CT_x, V_2CT_x, Nb_2CT_x, $Nb_4C_3T_x$, $Ta_4C_3T_x$, $(Mo_{2/3}Sc_{1/3})_2AlC$, $Hf_3C_2T_x$ and dozens are possible according to computational studies.[11,47–52] MXenes have a standard expression, $M_{n+1}X_nT_x$, in which "M" is the early transition metal atom *e.g.* Ti, Nb, V, *etc.*, "X" is the carbide and/or nitride, and "T_x" represent the surface terminations. While $n = 1, 2, 3$ represents the number of layers thus forming 21, 32, and 43 structures of MXenes.[11] So far, MXenes have been synthesized *via* top-down approach from MAX precursors through a wet chemical etching route.[53–55] Mixed acid reactions (HF + HCl),[53,56,57] etching in fluoride salts (HCl + LiF, known as minimally intensive layer delamination (MILD) method),[58,59] water-free etching in polar solvents.[60] Some alternative methods such as fluoride-free alkali etching,[61–63] halogens based etching[64,65], and solid-state etching using molten salts,[66–68] have also been employed to produce MXenes but most of them are etched by using different solutions of HF acid. Usually, the MAX powder is immersed in HF-contained solutions during the etching process under continuous stirring,[69] while temperature, reaction time, and HF concentration are the key parameters.[11,70] Nb_2C MXene, for example, is obtained by etching Nb_2AlC MAX powder in 48–50% concentrated HF solution at 55 °C for 40 hours under continuous magnetic stirring followed by a washing step.[51] The advantages of using a fluoride-based etching method are its accordion-like structure and small flakes, but the disadvantage is its high toxicity and hazardous nature. Alkali etching, for example, does not require fluoride-containing acids, but certain oxides or hydroxides can inhibit the removal of aluminum, which affects the quality of MXenes. Hence, subject to the preferred quality of MXenes and the final application, there are many ways to its synthesis. A schematic illustration of wet chemical etching through direct delamination with the MILD method (route-1) and molten salt etching (route-2) is explained in Fig. 1a. After etching, the product consists of a few nanometres thick multilayer MXene sheets (ML-MXene) with a large lateral size down to a few microns. ML-MXenes can subsequently be delaminated into few (FL-MXene) or single layers (SL-MXene) by intercalation of different organic molecules.[71,72] The nature of bonds between MX layers is mixed ionic, covalent, and metallic while the bond between MA layers is only metallic.[73] Due to this difference in relative intensities of the bonds and reactive nature with fluoride-contained solutions, it is possible to selectively remove the interleaved "A" layer chemically. One of the initial analyses to confirm the formation of MXenes is to compare its XRD spectrum with the corresponding MAX phase. Significant differences in the XRD spectrum after conversion of the MAX phase to the corresponding MXene can be seen in Fig. 1b (left). The XRD spectrum of the MAX phase in Fig. 1b(I) shows several well-defined crystallographic peaks that are significantly disappeared (after etching) in the case of $Ti_3C_2T_x$ MXene as shown in Fig. 1b(II). Typically, the peak at 2θ around 39° which corresponds to the "Al" disappears, while (00l) peaks become broader and downshifted at lower angles. The former represents the successful removal of "Al" from the MAX phase, while the latter represents an increase in *c*-LP, thus confirming the formation of multilayers MXene. Observe that only (00l) peaks are present in wet multilayers of $Ti_3C_2T_x$ MXene and/or properly delaminated $Ti_3C_2T_x$ MXene films due to the in-plane alignment of MXene flakes (Fig. 1b(III and IV)). Because of layered structure and hydrophobicity, external species (*e.g.*, H_2O, Li^+ ions, *etc.*) can intercalate into MXene sheets and alter the interlayer spacing. It is, therefore, crucial to understand the differences between *c*-LP, *d*-spacing, and interlayer spacing. The rights side of Fig. 1b demonstrates the basic notion of various lattice parameters which may be misleading in some cases when discussing the structure of MXenes. Scanning electron microscopy (SEM) image of Ti_3AlC_2 MAX is presented in Fig. 1c(i), While the SEM image of corresponding $Ti_3C_2T_x$ MXene in Fig. 1c(ii) shows typical accordion-like morphology of MXenes, which is another indicator of MXenes formation. Raman analysis can be utilized to characterize 2D materials, and studies have also been performed on

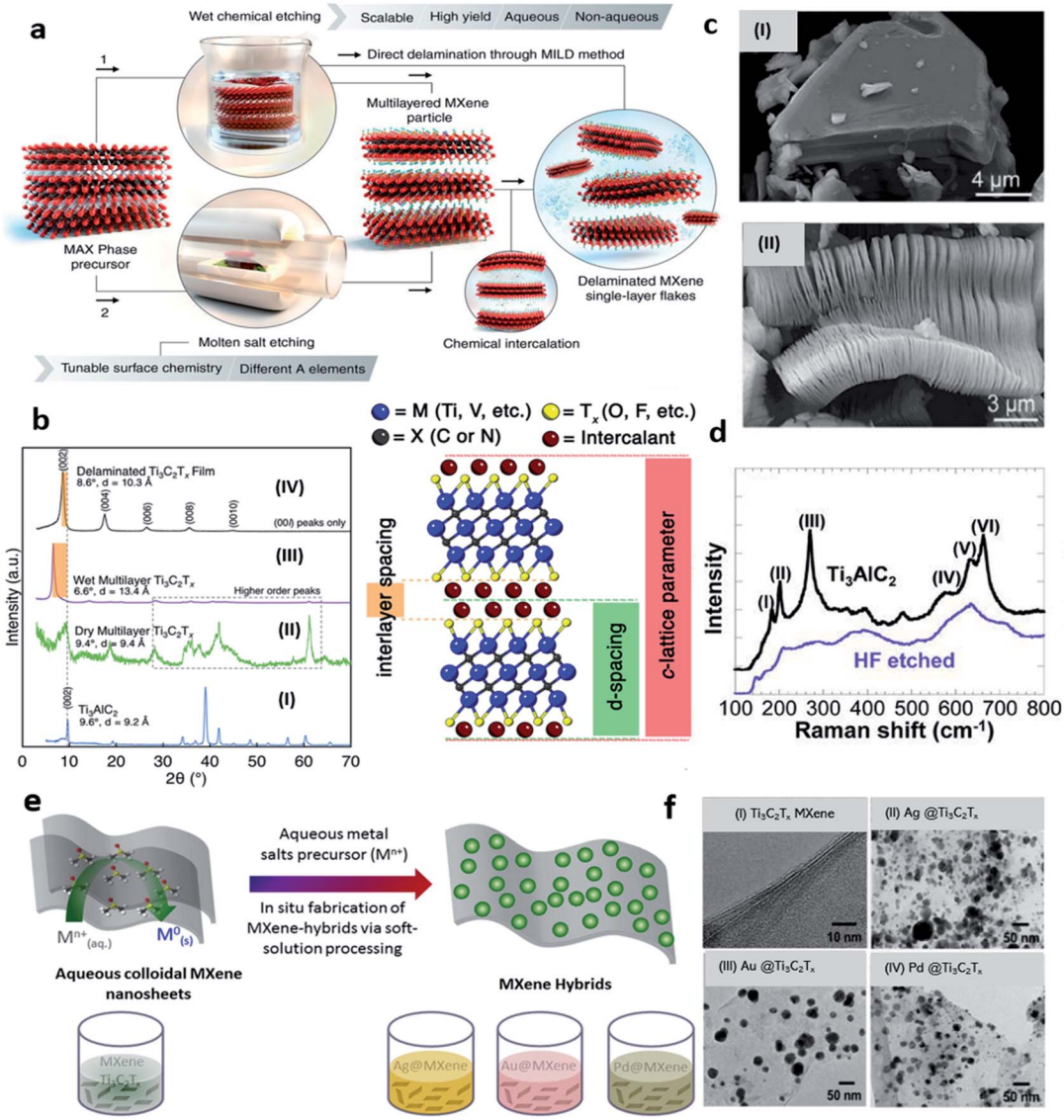

Fig. 1 (a) Schematics of different etching routes of MXenes and depiction of subsequent intercalation and delamination steps, reprinted with permission from AAAS.[83] (b) X-ray diffraction (XRD) spectrum of (I) Ti_3AlC_2 MAX phase, (II) dry multilayer MXene, (III) wet multilayers $Ti_3C_2T_x$ MXene, and (IV) LiCl delaminated $Ti_3C_2T_x$ MXene. The difference between interlayer spacing, *d*-spacing, and *c*-LP (lattice parameter) with two layers of intercalant (*e.g.*, H_2O, Li^+ is presented in the schematics on the right side of (b)). Adapted after permission from ref. 84 copyright© 2021 Elsevier. (c) SEM images of (i) Ti_3AlC_2 MAX and (ii) $Ti_3C_2T_x$ MXene with typical exfoliated graphite-like morphology. Adapted after permission from ref. 85 copyright© 2012, American Chemical Society. (d) Raman spectrum of $Ti_3C_2T_x$ before (upper curve) and after HF etching (bottom curve). Adapted after permission from ref. 11 copyright© 2011 WILEY-VCH Verlag GmbH & Co. KGaA, Weinheim (e) schematic illustration of Ag, Au, and Pd@MXene ($Ti_3C_2T_x$) hybrids formation by soft-solution processing. (f) TEM images of (i) $Ti_3C_2T_x$, (ii) Ag@$Ti_3C_2T_x$, (iii) Au@$Ti_3C_2T_x$, and (iv) Pd@$Ti_3C_2T_x$ nanohybrids. Adapted from ref. 86 under the terms of the CC-BY license, copyright© 2016, the authors, published by nature scientific report.

MXenes. Raman spectra of Ti_3C_2 MXene before and after HF treatment is shown in Fig. 1d. The peaks at positions I to III are attributed to Al–Ti vibrations and peaks at V and VI ascribe Ti–C vibrations. After etching, only Ti–C peaks are retained while Al–Ti peaks are disappeared which shows an effective loss of Al. The shifting and widening of the spectral lines are also consistent with the behaviour of peaks observed in XRD.[11] Based on elemental composition and etching techniques, outer layers of MXenes are terminated by different functional groups *e.g.*, oxygen (–O), fluorine (–F), and hydroxyl (–OH), as predicted by many theoretical studies.[74–76] Instead, MXenes have mixed surface terminations on their surface when etched with fluoride and chloride-containing acidic solution.[70,73,77–79] These functional groups are randomly distributed on the surface of the MXene layers. According to scanning transmission electron microscopy (STEM) studies, F-atoms reside at face-centered cubic adsorption sites (fcc), whereas oxygen "O" initially resides at closed hexagonal sites (hcp), further rearranged into fcc-sites after vacuum annealing at high temperatures. In addition, thermal treatment can alter the elemental

composition and coordination of surface functional groups.[75] This suggests that the MXenes have tunable chemistry and provide significant control over their physical properties. Oxygen terminations are shown to be more stable than –F counterparts and vacuum annealing of $Ti_3C_2T_x$ MXene from 330 °C to 775 °C results in the removal of the –F functional groups. In addition, the de-functionalization of the –F terminations shows improvements in the conductivity of the $Ti_3C_2T_x$ MXene.[80,81] Furthermore, the chemical structure of MXenes can also be transformed by intercalation of organic molecules.[81,82] In this process, suitable intercalating molecules are introduced during a mixing step followed by sonication, and centrifugation is executed to separate the delaminated MXene from the non-delaminated one.[54] The resultant suspension contains an electrostatically stable colloidal form of MXenes that is further processable depending upon the final applications.[87] As a matter of fact, all the approaches depend on the etching method, the type of intercalant used, and the required concentration of MXene colloidal.

MXenes supremacy

It is crucial to understand what makes MXenes so important in biosensing applications than other 2D materials! Having a variety of "M" and "X" elements with abundant surface terminations, MXenes have diverse properties that can be tuned to address a spectrum of applications. Many approaches such as surface and interlayer engineering, doping, and synthesis of MXenes heterostructures have been followed to alter the properties of MXenes.[88,89] Synergistic additive-mediated intercalation and chemical modifications notably change the physical nature and properties of MXenes.[90] For instance, alkali cation intercalation can modify the *c*-LP while intercalation of small molecules (*e.g.*, urea) delaminates the MXenes into a few layers. As discussed previously, Hart *et al.* have pointed out that the surface termination engineering has improved the electronic conductivity of MXenes, and intercalation induces a transition from metal to semi-conductor-like transport.[81] MXenes hold a unique combination of various promising features such as the presence of redox-active sites, high anchoring capacity for biomaterials and rapid transduction of electrical and optical signals.[91,92] Such factors play a pivotal role to realize ultrasensitive biosensors with high specificity and significantly low limits of detection (LOD). MXenes can host several target-specific biomolecules (*e.g.*, antibodies, enzymes, aptamers, *etc.*), which may contribute to the specificity of MXene-based sensors. Furthermore, MXenes provide a strong chelation interaction with DNA which is another aspect of achieving high specificity. This signifies that the MXenes provide favourable conditions for modifying the sensing assembly to achieve high specificity. MXene's large surface area and ample surface terminations provide a large capacity to immobilize bio-recognition elements. So, intrinsic surface terminations of MXenes can be utilized to further improve the performance of biosensors. For example, functional groups offer more ammoniation in NH_2 modified Ti_3C_2 MXene (NH_2–Ti_3C_2), hence providing more active sites for catalytic reduction that subsequently increases the sensitivity toward cardiac troponin-I (cTnI) detection.[93] Typical electrochemical transducers suffer from certain limitations such as low charge mobility due to poor conductivity, long detection times due to low mass transfer rate, and high overpotential requirements due to small effective surface. MXene can overcome these common attributes due to its fast charge kinetics while its large surface area can increase mass transfer and offer small electroanalytical overpotentials. MXene provides less current leakage as compared the graphene in an off state thus providing high detection sensitivity.[94] Furthermore, the properties of MXenes depend both on the transition metal atoms "M" and the number of layers "*n*" they contain. Unlike Ti_3C_2 MXene, which reportedly exhibits a strong interface coupling and increased charge mobility, V_2C MXene has a large surface area and thus have more active sites.[95] Moreover, layered morphology and the physical nature of the sheets can be further manipulated by various post-processing techniques.[84] These layers provide a significant protective microenvironment to the entrapped biological elements where they can remain stable and retain their biological activities.[96] MXenes good solution dispersibility can be utilized to manufacture electrodes for electrochemical sensors *via* the drop-casting technique, and their adaptable rheological nature makes them feasible to fabricate complex architectures and print various industrial devices using MXene ink, for example.[87,97] Since $Ti_3C_2T_x$ MXene is strongly hydrophilic, it possesses excellent antifouling potential, which makes it effective in passivating the biofouling effects; thus, $Ti_3C_2T_x$ MXene is a perfect model for the applications in electrochemical biosensors.[137] MXenes also have versatile electronic properties including tunable bandgaps, which result in tunable transmittance and absorption properties.[98] As Surface Plasmon Resonance (SPR) and Surface-enhanced Raman Scattering (SERS) offer ultrasensitive detection with reasonably low limits. Due to its extraordinary optoelectronic nature, the use of MXenes in the construction of such sensing platforms can greatly improve the sensitivity and limit of detection even at low target concentrations. Moreover, Double Transition Metal MXenes (DTM) have also been synthesized in which two different transition metal atoms reside at M-sites with in-plane and out-of-plane ordering.[99,100] These structures are more stable than conventional single M-atom MXenes "mono-MXenes" and offer chemical diversity and tailorable electrochemical properties.[100] Convincingly, MXene with its tunable physical and chemical properties appears to be a viable candidate for both electrochemical and optical biosensors. Furthermore, nanoparticles can improve the biosensing profile of MXenes with a good figure of merit, which will be discussed in the later sections.

Challenges associated with MXenes and possible solutions

Despite being dominant over other 2D materials for biosensing applications, there are certain challenges associated with MXenes. Long-term stability of nanostructures with a minimal

degradation rate is crucial in the development of biosensors and improving the clinical diagnostics. In contrast, MXenes get oxidized when produced in an aqueous media. So, their long-term stability is essential. HF-etched MXenes are less stable and easily oxidized under ambient conditions. Elevated temperature, dissolved oxygen, and aqueous medium can significantly increase the kinetics of MXenes oxidation. Degradation of MXenes in colloidal solutions can be prevented by introducing an argon environment and storing at a low temperature can further increase their stability.[101] Since, the edges of the sheets are prone to water molecules and/or dissolved oxygen than the base surface so MXene's oxidation starts from there. Edge capping with polyanionic salts, such as polyphosphate, improves the stability of MXenes, and studies have shown that the MXene after edge capping showed no oxidation.[104] However, this study lacks a thorough examination of the effects of introducing ionic salt to the conductivity of the MXene and this needs to be addressed more in detail. Similarly, the defects in Ti_3C_2 MXene sheets can instigate oxidation.[106–108] According to recent studies, modification in the synthesis route of the MAX phase using a higher stoichiometric amount of "Al" during the synthesis of MAX phase precursors enhances the oxidative stability of MXenes. This involves higher "Al" in MAX phase synthesis (double than conventional Ti_3AlC_2 MAX phase) and the MXene nanosheets produced from such MAX are termed as Al–Ti_3C_2. However, it is essential to wash of MAX phase with HCl to remove the dissolved intermetallic impurities before MXene synthesis. MAX phase synthesized by using excess "Al" contents has a smaller number of defects in its carbon sublattice which results in less defective MXene. Taking that into consideration, fewer defects in the structure of MXene lead to less possibility of its oxidation and increases the shelf life which is a crucial factor in the stability of MXene-based biosensors and realizing its commercial applications.[34] Reactive force field (ReaxFF) based molecular dynamics simulations suggest that the oxidation of $Ti_3C_2T_x$ MXene depends on the storage conditions such as temperature and concentration of oxidants.[109] Effect of temperature has a positive correlation with MXenes oxidations as the increase in the temperature increase the rate of oxidation. At high temperatures, carbon and TiO_2 is formed at the edges and transform Ti_3C_2 monolayer MXene flakes into TiO_2/carbon hybrid material.[110] Aqueous solution of Ti_3C_2 completely changed into TiO_2 anatase and the colour of MXene dispersed solution shifted from black to transparent white.[103] Moreover, flakes size has a negative correlation with the rate of oxidation *i.e.*, the smaller the flakes are the higher will be their oxidation kinetics. The adsorption of O_2 *via* under-coordinated Ti atoms initiates the oxidation of Ti_3C_2 MXene flakes. So, water is not a compatible medium to store MXene.[111] Moreover, Chae *et al.* have pointed out the factors affecting MXenes oxidation into TiO_2 and investigated the corresponding gas sensing performance.[112] The adsorption of organic contents on the surface of MXene sheets and/or the intercalation of organic species constrained the diffusion of gas molecules. Both the cases lead to a low gas response and prove detrimental to the performance of the proposed sensors. Several promising studies have been performed on the utilization of TiO_2 nanostructured compounds for sensing.[113,114] TiO_2 NPs loaded Ti_3C_2 MXene with an organ-like structure have been used for haemoglobin (Hb) immobilization to fabricate a mediator-free biosensor for H_2O_2 detection. The proposed sensing device (Nafion/Hb/TiO–Ti_3C_2/GCE) showed an exceptional performance with significantly very low LOD of 14 nm, a broad linear range of 0.1–380 μM for H_2O_2 and a sensitivity of 447.3 μA mM^{-1} cm^{-2}.[115] Table 1 summarizes recent studies on the behaviour of MXenes oxidation and storage conditions. The oxidation stability of MXenes can further be improved by combining them with different nanomaterials. The integration of nanoparticles can prevent the interaction of oxygen with MXene flakes and could play a role as a sacrificial interface that can increase MXenes stability. Similarly, the inclusion of metal nanoparticles or other interlayer spacers such as CNTs can maintain the hexagonal stacking of sheets and provide more conductive pathways for electron diffusion with less interfacial

Table 1 Recent findings on MXenes oxidation stability and storage environment

MXene	Etching route	Storage conditions	Temp.	Stability	Ref.
Ti_3C_2	LiF + HCl	Under Ar-atmosphere	5 °C	4 weeks	101
		Dispersed in NaAsc	RT	3 weeks	102
		Dispersed in IPA in O-atmosphere	RT	4 weeks	103
		Dispersed in IPA in Ar-atmosphere	RT	4 weeks	103
		Freezed aqueous solution	−18 °C & −80 °C	10 weeks	103
		Edge capping *via* polyanions salt[a]	RT	3 weeks	104
		Coating MXene films by ZIF-8	RT	30 days	105
V_2C	50% HF	Edge capping *via* polyanions salt[a,b]	RT	3 weeks	104
	HF + HCl	Salt exchange method[c]	RT	Up to 3 month	102
Ti_2C	LiF + HCl	Under Ar-atmosphere	5 °C	10 days	101
	LiF + HCl	Dispersed in IPA in O-atmosphere	RT	3 days	103
	LiF + HCl	Dispersed in IPA in Ar-atmosphere	RT	3 days	103

Abbreviations: Ar = argon, NaAsc = sodium L-ascorbate (antioxidant), IPA = isopropanol, ZIF-8 = zeolitic imidazolate framework (ZIF-8).[a] Edge capping of Ti_3C_2 and V_2CT_x MXenes using polyphosphates, polysilicates, or polyborates salts. [b] V_2C is the least stable MXene in its powder form. [c] Adding excess LiCl into V_2C suspension creates flocculation and improves its stability up to months.

resistance. The instability of Ti_3C_2 MXene under anodic potential is another challenge. Ti_3C_2 nanocomposites with metal nanoparticles *e.g.*, Pd and Pt overcame this instability.[116,117] In addition, bare MXenes are unstable and can easily form aggregates in physiological media. Various polymer-based surface modification strategies are applied to Ti_3C_2 and Nb_2C MXenes, including polyethylene glycol (PEG) and polyvinyl pyrrolidone (PVP) that can prevent the aggregation of these materials.[118–121] However, many of the issues with MXene arise from their synthesis protocols. Surface terminations also affect the biocompatibility and limit the use of MXenes for some applications. For instance, MXenes with –F terminations on their surface tend to release HF during the electrochemical reaction (*e.g.*, hydrolysis), which can significantly damage the normal tissue and obstruct enzyme activities. So, fluoride-free synthesis routes are required and similar methods are addressed in later sections.

MXenes: a distinctive matrix for nanoparticles loading

MXenes serve as a supporting substrate for *in situ* growth of nanoparticles *via* chemical reduction of precious metal salts. This brings an extra feature to MXenes in tailoring their biosensing profile. MXene surfaces can also be modified through electrostatic adsorption and incorporating metal nanoparticles to enhance their biosensing profile. Gold nanoparticles are highly regarded for their optical properties, biocompatibility, and ability to synthesize into various shapes while Ag, Pt, and Pd nanoparticles are also common. According to Li *et al.*, the size of AuNPs on the MXene surface, as well as the catalytic performance of such composites, can be controlled by controlling the self-reduction reaction time in $HAuCl_4$ solution at room temperature.[122] Studies have shown that MXene acts as a substrate for NPs loading, hence avoiding their loss or agglomeration whereas NPs can also maintain the layered stacking of MXene sheets.[86,123] Rakhi *et al.* have reported an amperometric biosensor by effective immobilization of glucose oxidase GO_x on Nafion solubilized Au/Ti_3C_2 nanocomposite (GO_x/Au-MXene–Nafion/GCE) for glucose sensing. Practically, $HAuCl_4 \cdot 3H_2O$ solution (0.075 M) was used as AuNPs precursor, and a mixture of 0.1 M $NaBH_4$ and 1 M NaOH as reducing agents. After Ti_3C_2 addition, the mixture was ultrasonically treated. The synergic effects between MXene sheets and AuNPs give rise to improved electrocatalytic behaviour, and the sensor shows relatively better sensitivity (4.2 μA mM^{-1} cm^{-2}) and a lower LOD (5.9 μM).[124] Similarly, AuNP@$Ti_3C_2T_x$ amperometric biosensor was reported for the determination of uric and folic acid showed a limit of detection of 11.5 nM and 6.20 nM respectively.[125] An amperometric biosensor based on AuNPs/Ti_3C_2 for nitrite ions detection shows a good anti-interference ability and suitability for nitrite ions detection with LOD (0.14 μM) and high sensitivity (0.0062 μA μM^{-1}).[123] Since, these reports focus on Ti_3C_2 MXenes, details about the synthesis of AuNPs composites with Ti_2C MXene can be found in the literature.[126] Delamination and formation of a stable colloidal suspension of MXenes is crucial in many of its applications. An essential way to employ MXenes in a biosensor is to cast/coat its dispersion on the electrode and/or substrate surface and follow the subsequent immobilization procedures. Delamination of MXene in bovine serum albumin media (BSA) is a unique way to form its stable suspension.[127] Electrostatic interaction and hydrogen bonding between BSA molecules and functional groups in MXene results in the formation of stable colloidal suspension without disrupting the intrinsic chemical structure of MXenes. In addition, BSA provides a suitable biological environment for many biological processes. Besides Nafion, many studies have reported the use of chitosan (CS) to prepare a stable dispersion of MXenes or MXenes-NPs composites due to its biocompatibility and non-toxicity. Chitosan provided a biocompatible environment for the immobilization of enzymes, which in turn provides a favourable habitat for analyte detection. Moreover, amine groups of chitosan can covalently immobilize the biomolecules. For example, AChE immobilized CS-dispersed-Ti_3C_2 MXene sensing platform (AChE/CS–Ti_3C_2/GCE) is reported for malathion detection.[128] Further modification of Ti_3C_2 with metal nanoparticles can increase their activity in biosensing. Silver nanoparticles modified AChE-based Ti_3C_2 (AChE/CS–Ag@$Ti_3C_2T_x$/GCE) show an enhanced electrochemical signal and a lower LOD (3.27 fM) toward organophosphorus pesticides (OPs) detection.[129] Silver nanoparticles increase the electron transfer and enlarge the surface area for OPs detection. In contrast, a mixture of AChE-CS was casted on the electrode interface and the sensors composed of MOF-derived MnO_2/Mn_3O_4 hierarchical micro cuboid (AChE-CS/Ti_3C_2/AuNPs/MnO_2/Mn_3O_4/GCE) resulted in lower LOD (0.134 pM) towards OPs determination and better recoveries in real samples.[130] Besides the satisfactory performance and improved limit of detection, such electrochemical biosensors have certain disadvantages like high cost and complex synthesis routes. The negatively charged surface of MXenes can be modified *via* electrostatic adsorption of positively charged species such as polyethyleneimine (PEI). This protocol was further extended to immobilize DNA aptamers.[131] Following this, PEI can be a promising way to incorporate gold nanoparticles on negatively charged MXene surfaces. Wang *et al.* reported PDDA (poly dimethyl diallyl ammonium chloride) modified AuNP/$Ti_3C_2T_x$ amperometric biosensing platform (AuNPs/$Ti_3C_2T_x$–PDDA/GCE) for NO_2^- detection. Positively charged PDDA neutralizes the negative charges on Ti_3C_2 sheets and decreases repulsive electrostatic interactions with NO_2^- ions. Moreover, attractive electrostatic interactions between PDDA and NO_2^- ions further enhances the sensitivity (250 μA mM^{-1} cm^{-2}) and improved the LOD (0.059 μM).[132] Due to their outstanding physical properties, bimetallic nanoparticles have gained considerable attention in biosensing. The synergistic effects at the nanoscale between properties inherited from bimetallic nanoparticles lead to improved electrochemical properties as well as enhanced sensitivity and specificity.[133] Moreover, bimetallic nanoparticles exhibit biomimetic properties as they can be used as bio-recognition molecules. In addition, the ultra-thin MXene nanosheet surfaces act as natural reductants and support the nanoparticles. Hence, the intrinsic properties of MXenes, such

as conductivity and redox potential, coupled with the properties of bimetallic nanoparticles can provide promising bio-sensing devices. In addition, the ultra-thin MXene nanosheet surfaces act as natural reductants and support the nanoparticles. Hence, the intrinsic properties of MXenes, such as conductivity and redox potential, coupled with the properties of bimetallic nanoparticles can provide promising bio-sensing devices. Zhao *et al.* reported bimetallic Au–Pd/Ti_3C_2 composite as an electrochemical sensing platform for paraoxon detection. Au–Pd composite was prepared on $Ti_3C_2T_x$ modified SPE by the self-reduction method which was then coated with glutaraldehyde (GA) as a cross-linking agent before enzyme immobilization.[134] Similarly, bimetallic Pd–Pt/$Ti_3C_2T_x$ composites are also reported for dopamine (DA) sensing. MXene nanosheets serve as a conductive matrix for loading Pd–Pt nanoparticles, and the NPs were anchored on DNA adsorbed Ti_3C_2 nanosheets which facilitate the uniform dispersion of the MXene, even growth of Pd/Pt nanocomposites and, increased electrocatalytic activity.[135] However, this involves a comparatively difficult synthesis procedure and the use of expansive DNA biomolecules. Another study shows a relatively simple method to prepare Ti_3C_2 MXene biosensors without integration of nanoparticles for DA detection with a relatively low limit of detection of 3 nM compared to 30 nM with Pd–Pt composites.[136] Furthermore, the embedded nanoparticles can act as a connector to bind an excess number of antibodies, thus increasing its capacity further. As an example, Ti_3C_2 MXene modified with gold nanoparticle (AuNPs@Ti_3C_2/Au) drop-casted on screen-printed gold electrode shows an increased surface density of immobilized DNA and almost four folds enhanced electrochemical signal.[137] MXenes rapid charge conductivity, large surface area, and remarkable biofouling resistance results in sensitive multiplex electrochemical detection of miRNAs. Besides MXene's intrinsic potential for optical biosensing, the incorporation of nanoparticles can significantly increase the Raman coupling and scattering intensity which can further increase the sensitivity. Studies have been performed to demonstrate the enhancement characteristics of $Ti_3C_2T_x$ MXene by examining the Raman spectral bands of well-adsorbed salicylic acid on hydroxyl-terminated MXene film. Salicylic acid serves as a model molecule to study the SERS enhancement of MXenes and acts as an active SERS in the case of silver and gold nanoparticles but this molecule shows no adsorption in the visible range.[138] The magnetic nanoparticles allow the separation of CEA antigen using a magnet without any pre-treatment, hence making the use of the sensor easier. Researchers have also demonstrated Nb_2C and Ta_2C MXenes in SERS-based biosensors. These MXenes show better SERS performance and Nb_2C/Ta_2C heterostructures showed ability towards SARS-CoV-2 protein detection with low LOD as 5 nM.[139] However, such phases of MXenes are still less explored and need more attention. SERS performance of various MXene including Mo_2C, Mo_2TiC_2, Ti_3CN, and V_2C has been evaluated with significant enhancement factors (EF) of 8.95×10^5, 4.55×10^5, 3.67×10^5, 5.60×10^5 for 10^{-7} M concentration of rhodamine 6G dye as an analyte on MXenes substrate.[140] Strategy for one step *in situ* hybridization of Au, Ag, and Pd nanoparticles from their aqueous solutions on Ti_3C_2 MXene surface for SERS substrates (Fig. 1c) and corresponding TEM images has been demonstrated in Fig. 1d(i–iv).[86] Since SERS signals obtained from a single kind of NPs are weak for ultrasensitive detection, one of the strategies is to use bimetallic NPs which provide different advantages of individual nanoparticles within the same structure. Strong plasmonic coupling between the bimetallic NPs creates a gigantic local electromagnetic field (localized plasmons), which results in signal enhancement and helps to fabricate advanced plasmonic nanostructures.[141,142] Zheng *et al.* investigated Janus Au–Ag NPs modified Ti_3C_2 as a SERS substrate which integrates the high plasmonic effect of AgNPs and good stability of Au nanoparticles.[143] Medetalibeyoglu *et al.* probed the use of Fe_3O_4@Au magnetic nanoparticles (NPs) and investigated Fe_3O_4@Au-delaminated $Ti_3C_2T_x$ composite as a SERS magnetic substrate for carcinoembryonic antigen (CEA) detection (Fig. 2).[144] Theoretical modeling offers promising approaches to synthesize new materials for sensing applications with an aim of high sensitivity, selectivity, and stability. The primitive aspect in biosensing is the interaction between the analyte and sensing material which gives rise to changes in the physical properties which are detected in many ways depending upon the type of biosensors employed. In 2D materials, due to out-of-plane weak van der Waals's interaction, the physisorbed molecules on the surface change the concentration of carriers which causes a change in the electrical resistivity or optical absorption.[145] In addition, weak interactions provides a superior recovery rate of the substrate material, whereas in contrast, strong in-plane covalent bonding stimulates chemisorption which follows the charges transfer mechanism among adsorbent and adsorbate.[146] Studies have theoretically predicted that in the case of transition-metal dichalcogenides such as MoS_2, amino acids are reported to be weakly physisorbed.

Intriguingly, "Au" nanoparticle modified MoS_2 alters the nature of interaction with amino acids and demonstrated the co-existence of physisorption and chemisorption. This is due to the covalent interaction of amino acids with AuNPs and non-covalent linkage to the sheets.[147] Theoretical studies have also been performed on MXenes as well. According to density functional theory calculations, O-terminated Ti_2C MXenes adsorb amino acids effectively through weak interaction among M-atom of Ti_2C and N-atoms from amino acids showing suitability for amino acid sensing.[148,149] Hence, theoretical simulations can provide an effective pathway to explore the nature of the interaction involved and to predict the sensing profile. From a theoretical point of view, interactions involving charge transfer and orbital interactions are of paramount importance. It provides critical insight into molecular interactions occurring at the nanoscale and understanding the inherent physical mechanisms. Various computational methods can give valuable insights into adsorption kinetics, charge transfer, and changes in physical properties during the adsorption events. It is rather important to mention that the theoretical perspectives of MXene in biosensing applications are not yet well explored, however, some studies thoroughly elucidate the fundamentals of biosensing applications of 2D materials.[150,151]

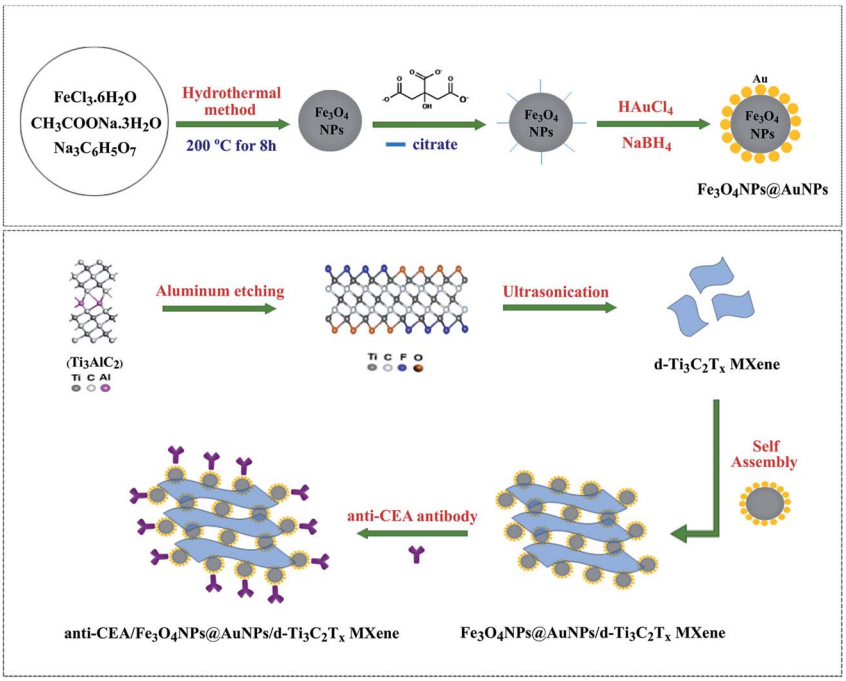

Fig. 2 Synthesis illustration of Au-coated magnetic nanoparticles and their self-assembly over MXene nanosheets. Reproduced from ref. 144 with permission, copyright© 2020 Elsevier.

MXenes in biosensing

MXene stands out as a promising material for biosensing applications among other 2D materials. The distinctive merits of MXenes in biosensing are their good biocompatibility and negligible cytotoxicity. Also, MXenes offer a wide adsorption spectrum for optical sensing and better interaction with DNA.[152,153] Several other factors are also associated with MXenes that can enhance the performance of MXene-based biosensors such as metallic conductivity, intrinsic surface functionalizations, and hydrophilic nature. Fig. 3 sums up all the paramount features of MXene that make them indispensable in biosensors. Ti_3C_2, among other compositions, has been widely reported. Few reports exist on other MXenes and their composites with metallic nanoparticles, especially in immunosensors. The purpose of this section is to discuss how the Ti-MXenes, as well as their nanocomposites with metal nanoparticles, can be used as electrochemical signal transducers and signal amplification tags in sandwich immunoassays. Then, we will highlight the applications of Nb-MXenes in different biosensors and HF-free etching methods.

Ti_3C_2-MXene in biosensing

Among the MXenes and titanium family, Ti_3C_2 is widely studied and reported in various applications including biosensors. As mentioned earlier, many reviews are published that cover various applications of Ti_3C_2 MXene in electrochemical and optical biosensors.[45,154–157] Herein, we aim to explicitly focus on the application of nanoparticles modified Ti_3C_2 MXenes in sandwich immunosensors and their function in various parts of such schemes. The large surface area of MXenes and numerous surface terminations can host an excess number of antibodies. Whereas the growth of nanoparticles not only provides more redox-active sites but enhances their effective surface area which in turn makes them more spacious and provides more binding sites to antibodies and results in an amplified signal. Sandwich immunoassay utilizes two antibodies, the capture/primary antibody (Ab_1) which is highly specific to the type of antigen/analyte, is attached to the electrode surface and the secondary/detection antibody (Ab_2) binds the antigen/analyte of detection. An antigen is captured at a different epitope of the Ab_2 than the primary antibody. In this way, the analyte is sandwiched between two antibodies. A pictorial realization of such kinds of schemes is shown in the graphical abstract.

Ti_3C_2-MXene based electrochemical signal amplification in sandwich immunoassays

Mohammadniaei *et al.* reported a novel combination of amplification strategies based on AuNPs@Ti_3C_2MXene for electrochemical signal amplification coupled with duplex-specific nuclease (DSN)-based amplification for rapid detection of miRNAs in total plasma (Fig. 4).[137] Ti_3C_2 MXene modified with 5 nm gold nanoparticles (AuNPs@MXene/Au) was deposited on the screen-printed gold electrode (SPGE). AuNPs/Au electrode was fabricated in comparison with AuNPs@MXene/Au electrode, and both the electrodes were loaded with abundant thiolated ssDNA (termed as base,[21] base[141]) corresponding to the target miRNA-21 and miRNA-141. The surface density of

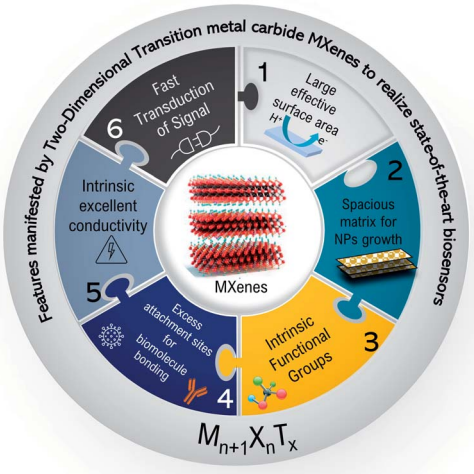

Fig. 3 Schematics representing the key features of MXenes concerning their applications in biosensing.

DNAs on AuNPs@MXene/Au electrodes was reported to be 3.45 times higher in magnitude as compared AuNPs/Au electrode. MXenes have a large effective surface area and ample surface terminations with a facile possibility to be externally modified, thus they can serve as an effective platform for biomolecules immobilization.[158–160] In addition to this, AuNPs supported by MXene nano sheets introduce thiol–Au bonding features, so that the observed increase in DNA surface density on AuNPs@MXene/Au can be ascribed to the well-distributed AuNPs within and on the MXene layers. In addition, the enhanced charged mobility and high electrocatalytic ability of MXenes elevates the electrochemical signal by four times. Moreover, AuNPs enhances the electrocatalytic performance of the electrodes other than introducing thiol-Au bonding features. Statistically, 15.7% of enhancement in amplified signal was attributed to the MXene intrinsic charge mobility and 84.3% increment was due to surface area expansion imparted by MXenes nanosheets, almost 3.57 times greater than AuNPs/Au electrode. The proposed sensors exhibit extraordinary selectivity with high sensitivity and specificity. Differential pulse voltammetry (DPV) responses shows distinct oxidation peaks of miRNA-21 and miRNA-141 individually, and in a mixture of different concentrations of miRNAs as well. This shows a high degree of selectivity and specificity of the proposed design (Fig. 5a). Due to nonspecific binding sites that inhibit DNA:DNA hybridization efficiency, AuNPs/Au electrodes showed 17% lower signal as compared to the electrode with MXene for the detection of 5 pM spikes of miR-21 and miR-141 in 10% human serum albumin (HAS) and Tris-buffer (Fig. 5b). The signals identified in the presence of MXenes indicate that the MXenes offer biofouling resistance in addition to signal amplification. The proposed assay showed a substantial LOD of 204 aM and 138 aM for miR-21 and miR-141 with a lower essay time of 80 minutes making it a significant design for point of care monitoring of cancer. Medetalibeyoglu *et al.* fabricated a MXene-based sandwich electrochemical immunosensors for procalcitonin (PCT) determination and examined the working of each component of the proposed sandwich scheme individually.[161] Sulfur-doped delaminated-Ti_3C_2 MXene (AuNPs/d-S–Ti_3C_2) modified with AuNPs (to utilize sulfur–gold affinity) was employed as a sensing platform. In addition to the enhanced surface conductivity provided by Ti_3C_2, the prepared sensing platform offers a wider surface for area primary antibodies (Ab_1) that are captured *via* AuNPs–amino interaction. The signal amplification probe was composed of carboxylated graphitic carbon nitride (c-g-C_3N_4) that carries secondary antibodies (Ab_2) through strong interaction between $-NH_2$ of the Ab_2 and –COOH bond of c-g-C_3N_4. The PCT antigen was captured *via* antigen–antibody interaction (Fig. 6a). c-g-C_3N_4 shows good electrocatalytic performance towards H_2O_2 and provides an amplified signal coupled with excellent conductivity of the MXene. Due to stable amidation between the carboxylic and

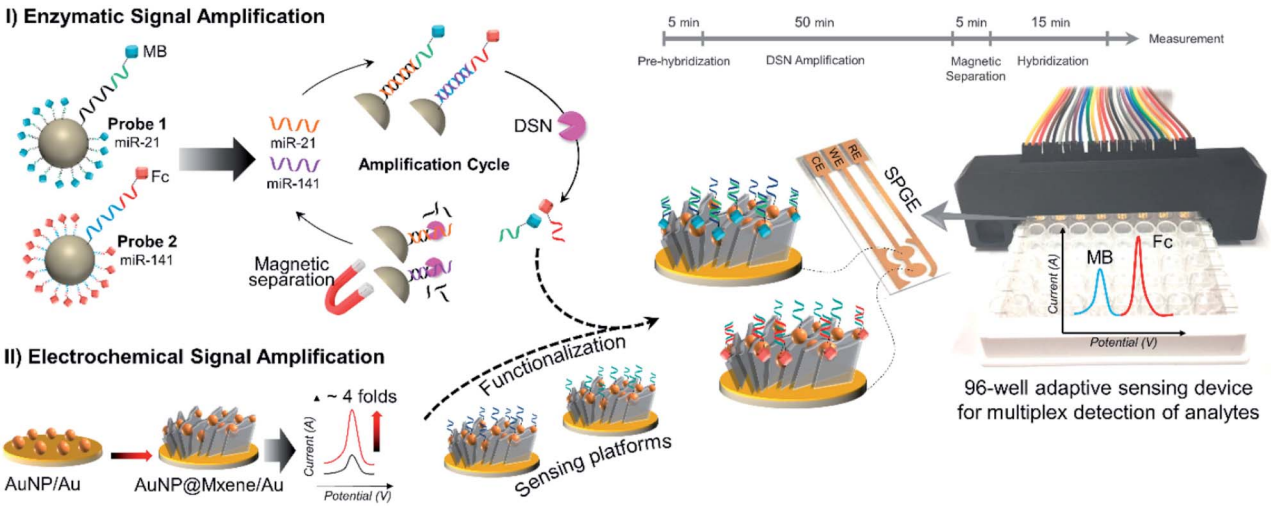

Fig. 4 Graphical illustration of magnetic particle (MPs) assisted enzymatic signal Amplification and MXene-based electrochemical signal amplification system for multiplex detection of miR-21 and miR-141. Reproduced from ref. 137 after permission, copyright© 2020 Elsevier.

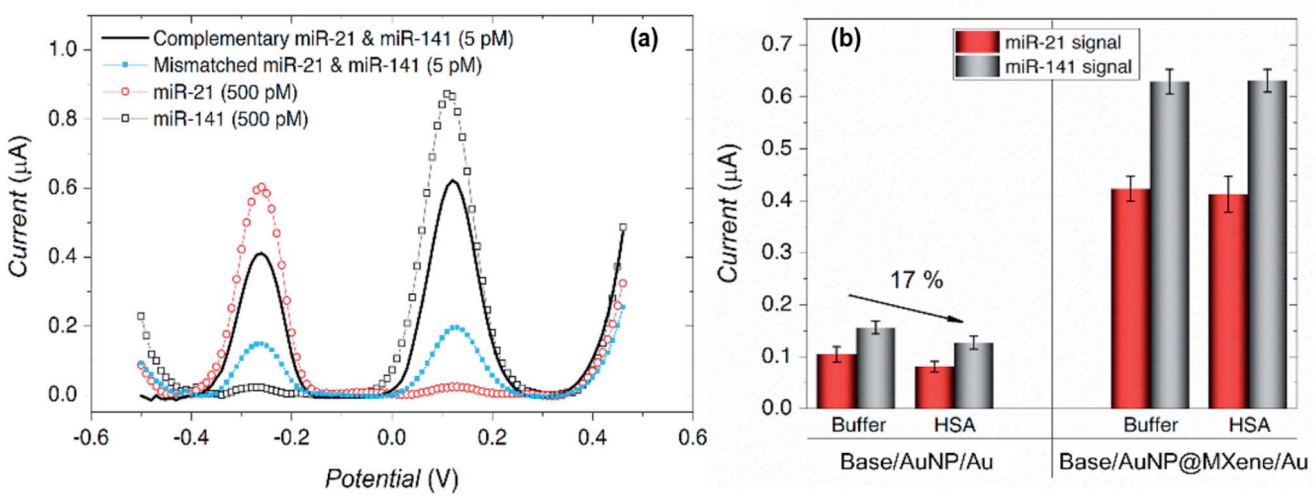

Fig. 5 (a) The developed sensors show a high degree of selectivity of the analytes in different miRNAs mixtures, while (b) shows the antifouling properties of MXene showing identical signal strength of the 5 pM miR-21 and miR-141 in 10% Human Serum Albumin (HAS) and Tris-buffer when compared with electrodes without MXene. Reproduced from ref. 137 after permission, copyright© 2020 Elsevier.

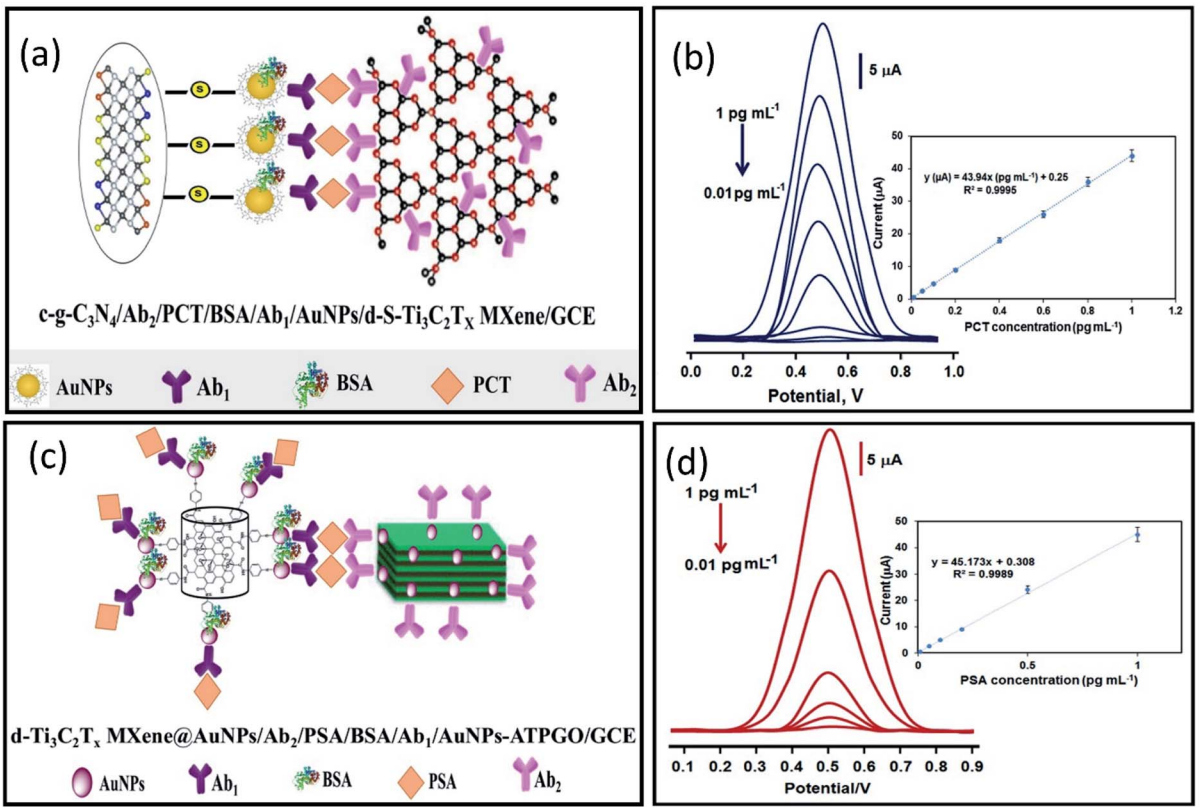

Fig. 6 (a) Schematics of immune interaction between Au-NPs functionalized d-S–$Ti_3C_2T_x$ MXene labelled with primary antibodies (Ab_1) as electrochemical signal transducers, and secondary antibodies (Ab_2) labelled carboxylated graphitic carbon nitride (c-g-C_3N_4/Ab_2) as signal amplification tag for PCT detection. Reproduced from ref. 161 after permission, copyright© 2020 Elsevier. (b) DPV signals show a linear relationship with PCT concentration (0.01 to 1.0 pg mL^{-1}) with a 2.00 fg mL^{-1} limit of detection. (c) Schematics of immune interaction between primary antibodies (Ab_1) labelled AuNPs–ATPGO/GCE as an electrochemical signal transducer and Au-NPs modified delaminated d-$Ti_3C_2T_x$ MXene labelled with secondary antibodies (Ab_2) as signal amplification tag for PSA detection. (d) DPV signals show a linear response with PSA antigen concentration (0.01 to 1.0 pg mL^{-1}) with a 3.00 fg mL^{-1} limit of detection. Reproduced from ref. 162 after permission, copyright© 2020 Elsevier.

amino group of c-g-C_3N_4 and Ab_2 respectively, c-g-C_3N_4 probe can carry numerous secondary antibodies (Ab_2) that can significantly enhance PCT antigen–Ab_2 interaction, which results in improved sensitivity. The proposed immunosensors show linearity between PCT concentration and immunosensor signals within a range of 0.01 pg mL^{-1} to 1.0 pg mL^{-1} and a LOD of 2.0 fg mL^{-1} with high selectivity among various interference agents and showed a stability up to 60 days (Fig. 6b). Prostate cancer is one of the most common cancers in men, but at the same time is curable when detected early, especially when it is localized. So, early diagnosis and monitoring of PSA concentrations are very important. Biosensors can provide a pathway toward the analytical detection of such diseases at early stages. A sandwich-type immunosensors for prostate-specific antigen (PSA) detection was designed by Medetalibeyoglu *et al.*[162] Sensing platform was fabricated of gold nanoparticles (AuNPs) and *p*-amino thiophenol (ATP) functionalized graphene oxide (GO) composite (AuNPs–ATPGO) loaded with primary antibodies Ab_1 *via* amino–Au affinity. After the PSA antigen was captured by Ab_1 *via* antigen–antibody interaction, d-$Ti_3C_2T_x$@-AuNP labelled with PSA–secondary antibodies (Ab_2) as a signal amplification probe was employed (Fig. 6c). MXene provides a large surface area for Ab_2 loading and, similarly stable interaction between gold atoms and $-NH_2$ of Ab_2 results in a stable and amplified signal. The proposed sensors exhibit a low limit of detection of 3.0 fg mL^{-1} with high selectivity and a wide linear range of 0.01 pg mL^{-1} to 1.0 pg mL^{-1} compared to other immunosensors developed for PSA determination (Fig. 6d).

Ti_3C_2-MXene based optical signal amplification in sandwich immunoassays

Surface plasmon resonance (SPR) emerges as a powerful optical detection technique for studying label-free biomolecular interaction in real-time with a variety of diverse applications. Due to its simplicity, many SPR instrument uses a detection scheme called the Kretschmann configuration which consists of a prism which is coated with a plasmonic metal layer onto its surface (most SPR sensors use gold) and shows variations in the refractive index during the event of biological reaction on the SPR chip (see Graphical abstract). The sensitivity of SPR sensors at low concentrations can further be increased by surface modification by metal nanoparticles.[163] Various studies have highlighted the theoretical characteristics of Ti_3C_2 MXene and unveiled their underlying sensitivity enhancement mechanism in SPR.[164,165] Wu *et al.* fabricated a sandwich-type SPR biosensor based on "Ti_3C_2/AuNPs as a sensing material" and multi-walled carbon nanotube-polydopamine (PDA)–AgNPs composite (MWPAg) as a signal enhancer for ultrasensitive detection of carcinoembryonic antigen (CEA).[166] To form a sandwich mechanism, monoclonal primary antibodies Ab_1 were immobilized on staphylococcal-protein-A (SPA) modified Ti_3C_2/AuNPs composite to capture analyte CEA and the polyclonal antibodies Ab_2 were conjugated with MWPAg that performs the role of signal enhancer (Fig. 7a). SPA can bind selectively with Fc regions of Ab_1 which enables an ordered and oriented immobilization of antibodies on the sensor surface, not simply the adsorption or covalent bonding. The proposed sensors show a linear response of relative resonant angle change ($\Delta\theta$) as a function of logarithmic CEA concentration and exhibit a low limit of detection of 0.07 fM with a broad concentration range from 2×10^{-16} M to 2×10^{-8} M (Fig. 7 b and c). The enhanced performance is attributed to strong electromagnetic coupling between dense AgNPs and underlying Au-chip is originated from dielectric changes due to antigen–antibody interaction events on the surface, thus increasing the refractive index of the chip. Moreover, the MWPAg signal enhancer probe noticeably amplifies the signal by increasing the mass transfer towards the sensing chip. Wu *et al.* further fabricated another Ti_3C_2 SPR sensor for CEA detection in human serum and provided a detailed analysis of signal amplification.[167] In the scheme as shown in Fig. 7d, amino-functionalized N–Ti_3C_2 MXene nanosheets were dispersed on Au-film as "a sensing platform" for covalent immobilization of monoclonal anti-CEA antibodies Ab_1 to capture target CEA analyte. As the hollow gold nanoparticles (HGNPs) can easily form aggregates because of the high surface energy, MXene confronts their aggregation and results in uniform distribution of HGNPs over its surface. HGNPS–N–Ti_3C_2 nanosheets were modified with staphylococcal-protein-A (SPA) to immobilize polyclonal anti-CEA antibodies Ab_2 (N–Ti_3C_2/HGNPs/SPA/Ab_2) and introduced to an SPR sensing system as a "signal enhancer". Due to strong plasmonic coupling between the inner and outer surface, HGNPs show an increase in the refractive index sensitivity as compared to solid gold nanostructures. Strong electromagnetic coupling between densely populated HGNPs and the underlying Au-chip increases the imaginary part of the refractive. Whereas N–Ti_3C_2/HGNPs/SPA/Ab_2 probe significantly increases the mass captured on the sensing chip that increases the real part of the refractive index of the chip surface. The sensor provides a broad detection range of 0.001–1000 pM, much larger as compared to similar studies on Ti_3C_2 MXenes and showed a LOD of 0.15 fM. Surface-enhanced resonance scattering (SERS) is another technique for sensitive detection of various analytes where MXenes can be used as a sensitive SERS substrate. The plasmonic nature of nanoparticles modified MXene hybrid nanostructures have been demonstrated by SERS and shows a high sensitivity towards methylene blue with an enhancement factor of 1.5×10^5, 1.17×10^5, and 9.61×10^4 for Ag@MXene, Au@MXene and Pd@MXene substrates, respectively.[86] Medetalibeyoglu *et al.* investigated sandwich immunosensors for CEA detection with 4-mercaptobenzoic acid (MBA) labelled MoS_2 NFs@Au NPs as SERS tag and Fe_3O_4@Au NPs–d-$Ti_3C_2T_x$ as SERS magnetic supporting substrate.[144] The magnetic nanoparticles allow the separation of CEA antigen from biological samples using a magnet without any pre-treatment, hence making the use of the sensor easier. The immunosensors principle is based on antigen–antibody interaction as depicted in the scheme (Fig. 8a). High intensities in Raman spectra at 1101 cm^{-1} and 1601 cm^{-1} can be observed in the case of this kind of sandwich-type immunoassay (Fig. 8b). These enhanced Raman intensities in this scheme are due to Fe_3O_4 NPs' super-paramagnetism that

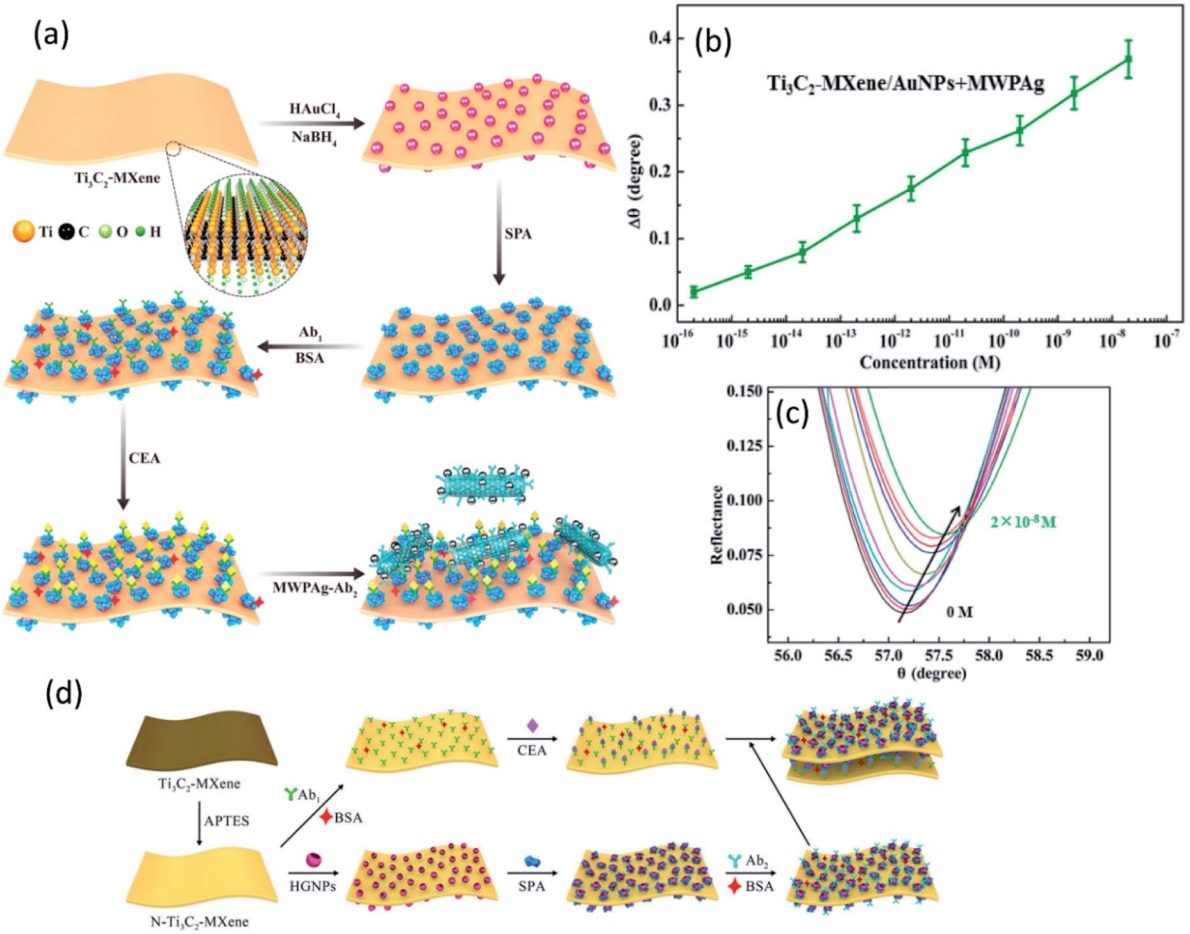

Fig. 7 (a) Illustration of fabrication mechanism of SPR biosensors based on standard Kretschmann configuration with MWPAg as signal enhancer tagged with secondary antibodies (Ab_2) and primary antibodies (Ab_1) immobilized Ti_3C_2-MXene/AuNPs sensing platform (b) the proposed sensors show a linear relationship of resonance angle shift ($\Delta\theta$) at different CEA concentrations. (c) Corresponding SPR spectra for CEA detection in concentration range 2×10^{-16} to 2×10^{-8} M. Reproduced from ref. 166 after permission, copyright© 2020 Elsevier. (d) Schematics of fabrication mechanism of SPR biosensors based on standard Kretschmann configuration with amino functionalized HGNPs decorate Ti_3C_2-MXene as signal enhancer tagged with secondary antibodies (Ab_2) and primary antibodies (Ab_1) tagged sensing platform. Reproduced from ref. 167 after permission, copyright© 2020, American Chemical Society.

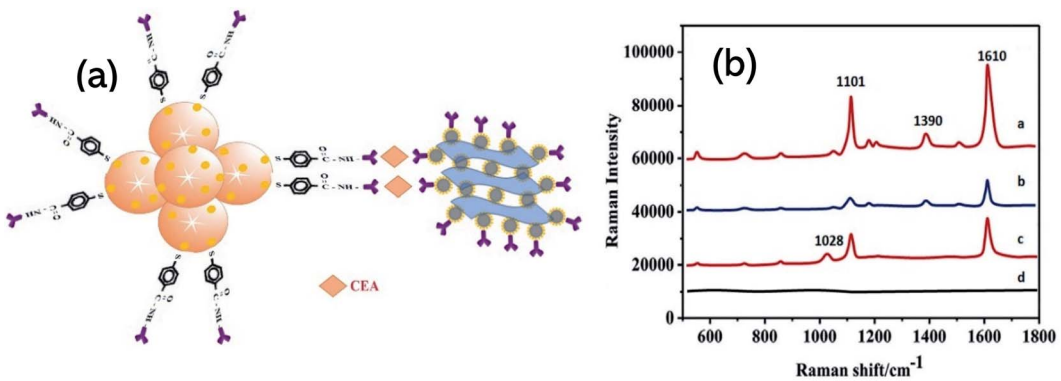

Fig. 8 (a) Schematic illustration of sandwich sensing assembly for CEA detection with SERS magnetic supporting substrate. (b) SERS spectra of MoS_2-NFs@AuNPs/MBA (spectrum-a), MoS_2NFs@AuNPs/MBA/anti-CEA (CEA SERS tag) (spectrum-b), sandwich type immunosensor including 1.0 ng mL^{-1} CEA (spectrum-c) and anti-CEA/Fe_3O_4NPs@AuNPs/d-$Ti_3C_2T_x$ MXene (spectrum-d). Reproduced from ref. 144 after permission, copyright© 2020 Elsevier.

Table 2 $Ti_3C_2T_x$ based sandwich schemes in sensing applications

Role of MXene	Detection method	Sensing platform	Analyte of detection	LOD	Linear range	Ref.
Sensing electrode material/substrate	SPR	MWCNTs-PDA–AgNPs–Ab_2/CAE/Ab_1–Ti_3C_2–AuNP–SPA@Au-film	CEA	0.07 fM	2×10^{-16}–2×10^{-8} M	166
	SERS	MoS_2 NFs@AuNPs/MBA/Ab_2/CEA/Ab_1/Fe_3O_4 NFs@AuNPs/d-$Ti_3C_2T_x$	CEA	0.033 pg mL^{-1}	0.0001–100 ng mL^{-1}	144
	DPV	c-g-C_3N_4/Ab_2/PCT/Ab_1/AuNPs/d-S-$Ti_3C_2T_x$/GCE	PCT	2 fg mL^{-1}	0.01–1.0 pg mL^{-1}	161
		Tb–Au–COF/Ab_2/CYFRA21-1/Ab_1/Au–$Ti_3C_2T_x$/GCE	CYFRA21-1	0.1 pg mL^{-1}	0.5–1 × 10^4 pg mL^{-1}	169
	SPR	N-Ti_3C_2/HGNPs/SPA/Ab_2/CAE/Ab_1/N-Ti_3C_2/Au-film	CEA	0.15 fM	0.001–1000 pM	167
		D-$Ti_3C_2T_x$@AuNPs/Ab_2/PSA/Ab_1/AuNPs–ATPGO/GCE	PSA	3 fg mL^{-1}	0.01–1.0 pg mL^{-1}	162
Signal amplification probe	DPV	AuNPs@MoS_2@$Ti_3C_2T_x$/Ab_2–Tb/CYFRA21-1/Ab_1/Nafion–AuNPs/GCE	CYFRA21-1	0.03 pg mL^{-1}	0.5 pg mL^{-1}–50 ng mL^{-1}	170
	ECL	Ti_3C_2–Apt_2/exosomes/Apt_1/PNIPAM–AuNPs/GCE	MCF-7 exosomes	125 particles μL^{-1}	5 × 10^2–5 × 10^6 particles μL^{-1}	171
		AuNPs–Ti_3C_2–Apt_2/exosomes/Apt_1/SA–PAM/GCE	HeLa cell line Exosomes	30 particles μL^{-1}	10^2–10^5 particles μL^{-1}	172
		AuNPs/Ti_3C_2–PEI/Ab_2/CEA/Ab_1/GR-IL-Pt/GCE	CAE	34.58 fg mL^{-1}	34.58 fg mL^{-1}	173

Abbreviations: Ab_1 = primary/detection antibody; Ab_2 = labelled/secondary antibody; NFs = nanoflowers; CEA = carcinoembryonic antigen, PSA = prostate specific antigen; PCT = procalcitonin; Tb = toluidine blue; CYFRA 21-1 = cytokeratin fragment antigen 21-1, GR-IL-Pt = graphene-ionic liquid-platinum; ATPGO = *p*-aminothiophenol (ATP) functionalized graphene oxide (GO) composite, c-g-C_3N_4 = carboxylated graphitic carbon nitride; SPA = staphylococcal protein A; COF = covalent organic framework.

creates local "hot spots" owing to improved conjunction of CEA SERS-tag to antigen. In SERS applications, the electromagnetic field in such localized plasmonic hotspots is intense and entitled to signal amplification. In addition to this, the peak at 1390 cm^{-1} in spectrum-a and the peak at 1029 cm^{-1} in spectrum-c (Fig. 8b) indicate according to literature that the sandwich structure was successfully fabricated and the prepared SERS magnetic immunosensor is feasible.[168] The proposed SERS magnetic immunosensor shows a linear response with CEA concentration and good stability up to 45 days. The sensors showed a LOD of 0.033 pg mL^{-1} towards CEA detection and expresses a wide range of detection from 0.0001–100 ng mL^{-1}. Table 2 encloses various Ti_3C_2 sandwich biosensors and their respective performance.

Ti_2C-MXene in biosensing

Though MXenes have been extensively studied, there are fewer studies regarding biosensing applications of Ti_2C MXene, particularly its composites with nanoparticles (*e.g.*, Au, Ag, *etc.*). Wang *et al.* have reported the synthesis of Ti_2C@Au core–shell nanosheets and examined their optical properties for photonic applications.[126] Regarding the environmental monitoring, Zhu *et al.* fabricated an Au–Ag nano shuttles (NSs) modified Ti_2C-based bifunctional nano sensing platform for electrochemical and SERS determination of ultra-trace carbendazim (CBZ) residues in tea and rice (Fig. 9).[174] Ti_2C/Au–Ag provides a wide surface area for electrochemical activities and synergistic electrocatalysis imparted by nanoparticles showed a low LOD of 0.002 μM. The electrochemical signal enhancement that can be seen in the scheme below can be attributed to the large surface and excellent conductivity of MXenes and chemical binding between Ti_2C and CBZ. A strong shift can be observed in Raman response with a considerable enhancement of the signal in the presence of Ti_2C/Au–Ag nano shuttles. This signal enhancement is ascribed to an intensive electromagnetic field due to localized plasmonic hotspots created by Au–Ag NS. Machine Learning *via* different algorithms such as Artificial Neural Network, support vector machine (SVM), and relevance vector machine (RVM) for the intelligent analysis of CBZ was employed. As compared to other approaches, RVM model provides the best fits with experimental data and displayed more superiority for intelligent analysis of CBZ. In addition, Ti_2C-based SPR sensors show an exceptional response to refractive index (RI) changes and detected trace concentrations of heavy metals in a time of less than one minute. So far, sensors based on Ti_2C-MXene are employed in environmental monitoring.[175]

Nb-MXenes in biosensing

Since the first report on its experimental synthesis, most of the research on niobium MXenes remained centered on energy storage. The excellent photothermal conversion ability in NIR-I and NIR-II bio-windows and cytotoxicity of niobium MXenes have led them to many biomedical applications.[118,176] However, their applications in the field of sensing are limited as compared to Ti_3C_2 MXene. To date, two phases of niobium

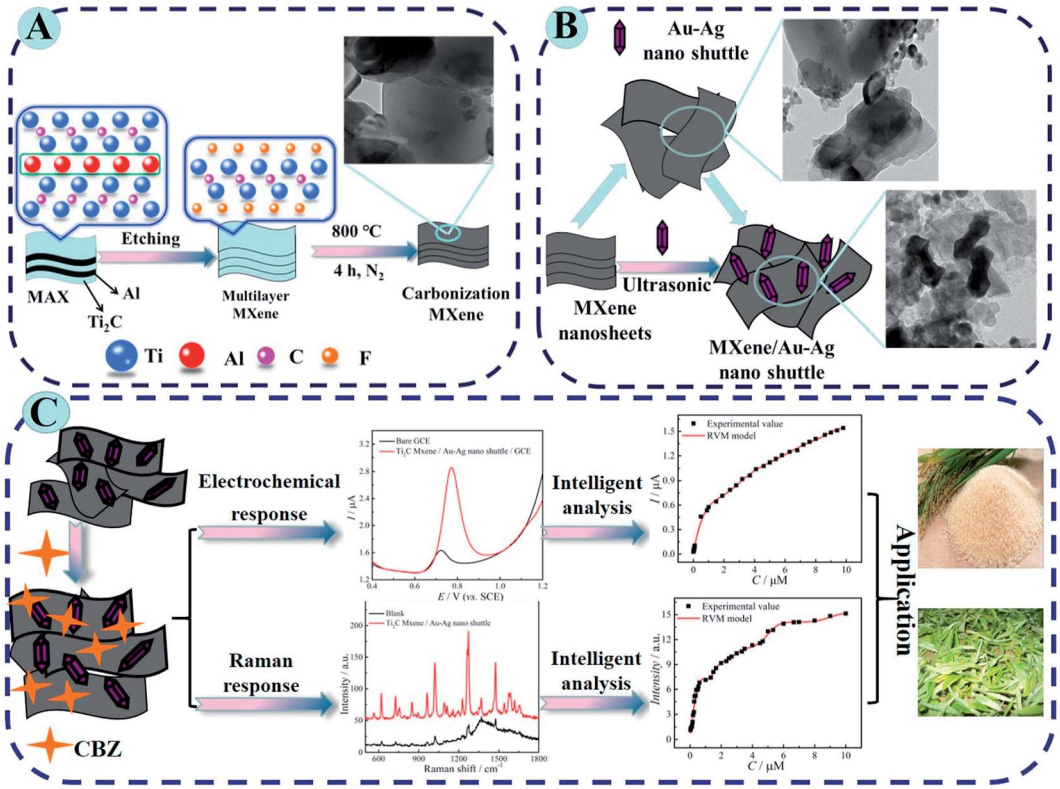

Fig. 9 (A) Synthesis of Ti_2C MXene and subsequent carbonization by annealing at 800 °C under nitrogen protection. (B) Schematic fabrication of Ti_2C MXene/Au–Ag NSs. (C) Experimental and theoretical studies of bifunctional biosensing platform for electrochemical and Raman analysis for CBZ determination in tea and rice residues. Reproduced from ref. 174 after permission, copyright© 2020 Elsevier.

MXenes are reported experimentally. Details of the synthesis and structural analysis of Nb_2C and Nb_4C_3 MXenes can be found in the literature.[51,52] Here, our focus is to highlight significant features of these phases and summarize their applications in biosensing. As discussed in detail in the previous sections, oxidation under ambient conditions is a common phenomenon associated with MXenes. However, the oxidative stability of Nb-MXenes is better than Ti-counterparts at room temperature, and it is gradual over time and can be further improved when stored at lower temperatures without antioxidants. Compared to Nb_2C MXene, Nb_4C_3 MXene shows improved oxidative stability since the higher the "n" value, the more stable the MXene becomes toward oxidation. Also, the presence of metallic phases and higher "n" in Nb_4C_3 makes it more electrically conductive than Nb_2C MXene. Applications of these MXenes in biosensors have emerged very recently. N. Arif *et al.* were the first to describe an Nb_2C MXene composite with ZnS nanoparticles for electrochemical sensing of dopamine (DA).[177] MXene's large surface area and electroactive sites of ZnS contributed to the sensitivity of the proposed sensing platform and offer a good selectivity in a mixture of ascorbic acid, citric acid, and glucose as interference agents. Compared to Nb_2C electrodes, Nb_2C/ZnS composite modified glassy carbon electrodes exhibit much better performance. Interestingly, the limit of detection was improved by almost 5 folds with Nb_2C MXene as compared to electrodes without MXene (7.24 μM for GCE/ZnS) and shifted to a lower value of 1.39 μM with a broad concentration range (0.09 mM–0.82 mM). In a relatively recent study, nitrogen, and sulfur co-doped Nb_2C MXene nanosheets (NS–Nb_2C) prepared using thiourea as an N,S source significantly improved dopamine sensing (DA) in gastric juice under acidic conditions (Fig. 10).[178] Large surface area and conductive network of MXene facilitate more electron transfer and provide enhanced conductivity. Heteroatom doping has significantly increased the Brunauer–Emmet–Teller (BET) surface area and increased defect concentration that provides more electrochemically active regions. The proposed sensor exhibits a limit of detection of 0.12 μM which is very less when compared with the ZnS modified Nb_2C sensor. This suggests that heteroatom doping is an efficient strategy to achieve sensitive detection. Among the niobium MXenes, Nb_4C_3 with its high electrical conductivity and with large intercalation capacity is expected to be more electrochemically active. Rasheed *et al.* reported that niobium-based MXenes are stable in an anodic potential window up to 0.5 V compared to Ti-counterparts and Nb_4C_3 MXene is more electrochemically active than Nb_2C.[179] This active electrochemical nature of Nb_4C_3 provides ultrasensitive detection of dopamine with a lower limit of detection of 23 nM as compared to the Nb_2C-based DA sensors previously discussed. There are certain other advantages associated with Nb_4C_3 MXene such as larger d-spacing and c-lattice parameter that facilitates the enhancement of its electrochemical performance. Pristine Nb_4C_3 exhibits good sensing performance towards Pb_2^+ detection in water with a detection limit of

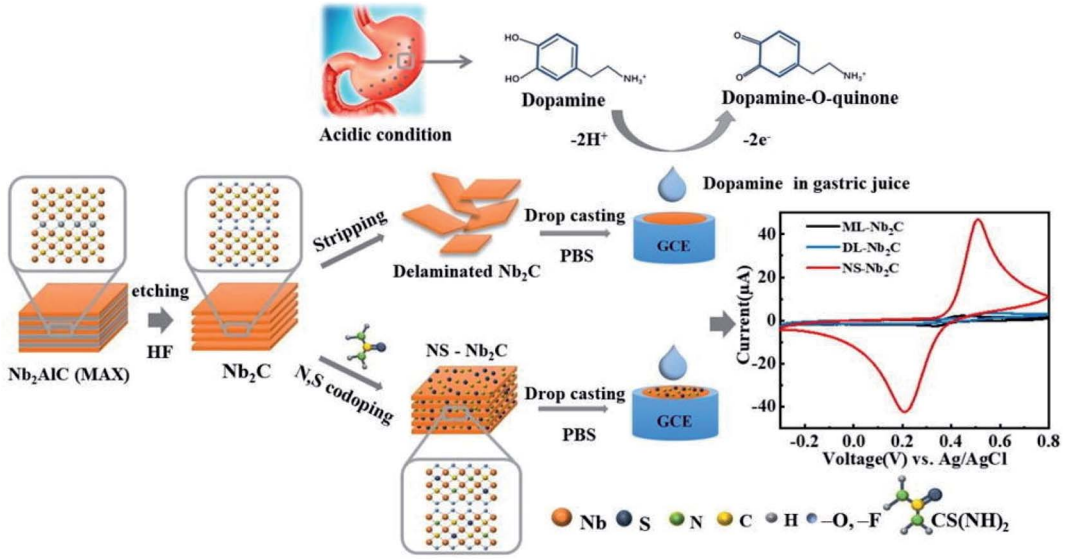

Fig. 10 Schematic synthesis of N,S co-doped Nb_2C MXene and assembly for DA sensing in acidic condition. CV curves on the right side shows that the redox current peaks in case of N,S co-doped Nb_2C sheets are greatly enhanced as compared to multilayered (ML) or delaminated (DL) Nb_2C MXene. Due to high electron transfer rate and surface area expansion for molecular interaction imparted by N,S doping. Reproduced from ref. 178 after permission, copyright© 2021 Elsevier.

12 nM.[180] The proposed sensor, however, utilized a deposition step to electroplate the working electrode and the performance was evaluated by measuring the reduction peaks through anodic stripping. However, AuNPs@Nb_4C_3 nanocomposite immobilized with (lead-specific) thiol-modified DNA (sDNA–Au@Nb_4C_3) showed a lower detection limit (4 nM) for Pb_2^+ ions in water. This lower limit is attributed to the self-assembly of thiol-modified lead-specific DNA with Au-modified Nb_4C_3-MXene through Au–S bonds and lead-binding DNAs.[181] To the best of our knowledge, as compared to Ti-counterparts, no studies have yet been published on Nb_2C MXene composites with metal nanoparticles, *e.g.*, Au@Nb_2C and/or Ag@Nb_2C, *etc.* Furthermore, their applications in electrochemical or optical immunosensors are found very limited, specifically in sandwich

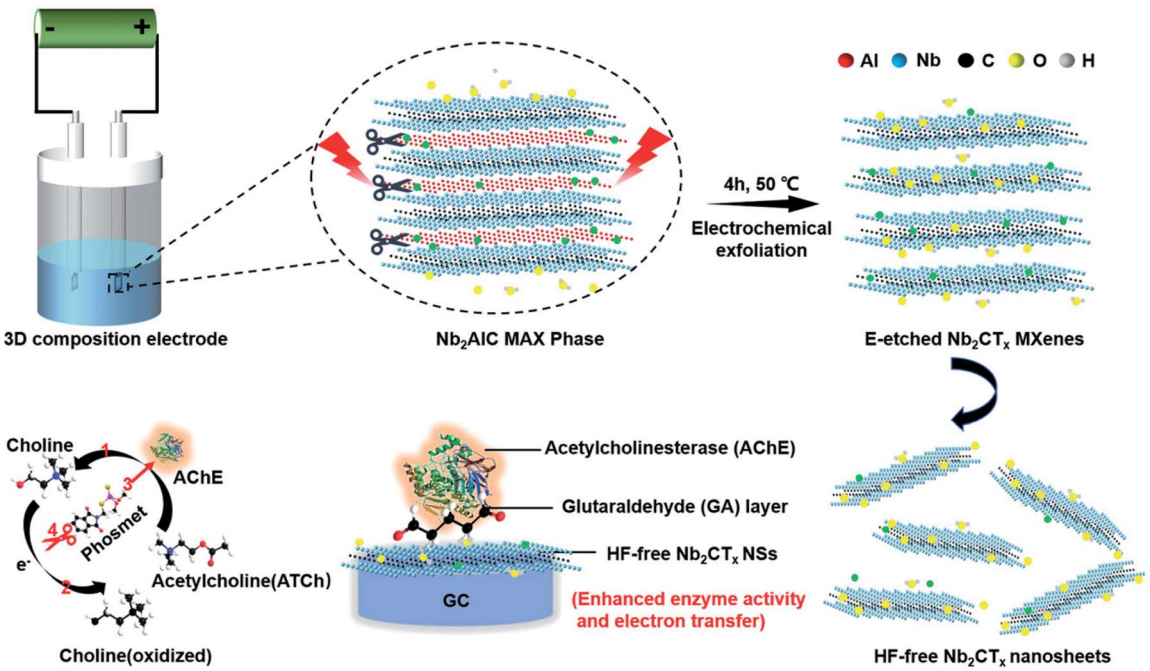

Fig. 11 Schematics for exfoliation and delamination process of Nb_2AlC MAX phase *via* electrochemical etching and the enzyme inhibition effect for phosmet detection by HF-free Nb_2CT_x/AChE based biosensor. Adapted under the terms of the CC-BY license from ref. 183, copyright© 2020, published by Wiley-VCH.

Table 3 M_2X (M = Nb, Ti, Ta) and Nb_4C_3 MXene in sensing applications

MXene	Detection method	Sensing platform	Analyte of detection	LOD	Linear range	Ref.
Nb_4C_3	DPV	$Nb_4C_3T_x$/GCE	DA	23 nM	10 nM–1 μM	179
		DNA–Au@$Nb_4C_3T_x$/GCE	Pb^{2+}	4 nM	10 nM–5 μM	181
	SWASV	$Nb_4C_3T_x$/GCE	Pb^{2+}	12 nM	0.10–0.55 μM	180
Nb_2C	DPV	N,S[a] co-doped-Nb_2C/GCE	DA	0.12 μM	0.4–90 μM	178
		Nb_2C–ZnS/GCE	DA	1.39 μM	0.09–0.82 mM	177
	CA	AChE/GA/HF-free Nb_2CT_x/GCE	Phosmet	0.046 ng mL^{-1}	0.2–1000 nM	183
	SERS	Nb_2C modified substrate	MeB	10^{-8} M	—	139
			MeV	10^{-6} M	—	139
	DPV	Ti_2C/Au–Ag NS[b]/GCE	CBZ	0.002 μM	0.006–9.8 μM	174
Ti_2C	SERS	Ti_2C/Au–Ag NS[b]	CBZ	0.01 μM	0.033–10 μM	174
	SPR	Ti_2C modified substrate	Pb^{2+}	79.2 ng L^{-1}		175
			Cr^{2+}	56.5 ng L^{-1}		175
			Hg^{2+}	92.8 ng L^{-1}		175
Ta_2C	SERS	Ta_2C modified substrate	MeB	10^{-6} M	—	139
			MeV	10^{-7} M		139

Abbreviations: GCE = glassy carbon electrode; LOD = limit of detection; DA = dopamine; CBZ = carbendazim; MeB = methylene blue; MeV = methylene violet; DPV = differential pulse voltammetry; CA = chronoamperometry; SWASV = square wave anodic stripping voltammetry; SPR = surface plasmon resonance; SERS = surface enhanced resonance spectra. [a] N,S = nitrogen and sulfur co-doped. [b] NS = nano shuttles.

immunoassays. However, it is important to mention that the Nb_2C–ZnO composite has been reported in sandwich-type electrochemiluminescence (ECL) biosensors for thyroglobulin detection.[182] Due to exceptional photothermal conversion performance, Nb_2C MXene acted as a thermal energy convertor to increase the temperature of electrode surface by converting laser energy into heat, and an efficient matrix for antibodies loading due to ample surface terminations and large effective surface area, that results in an amplified ECL signal. On the other hand, Nb_2C shows a remarkable SERS sensitivity with an enhancement factor of 3×10^6 and a low detection limit (10^{-8} M) towards MeB (Methylene Blue) molecule with 532 nm laser excitation.[139] However, etching in hydrofluoric-containing acidic solutions results in –F terminations on the MXene surface that limits their applications. Song *et al.* introduced an electrochemical etching strategy to obtain fluoride-free MXenes (Fig. 11).[183] To fabricate the sensing platform, glutaraldehyde (GA) was used as a cross-linking agent before AChE immobilization similar to what was reported in many earlier studies. Compared to the sensors based on HF-etched Nb_2CT_x MXene, fluoride-free Nb_2CT_x/AChE biosensor shows better performance for organophosphate pesticide (OPs) phosmet detection with a LOD of 0.046 ng mL^{-1} and provides certain advantages, such, low cytotoxicity, stable enzymatic activities, and superior electrochemical performance. Table 3 summarises the application of M_2X (M = Nb, Ti, Ta) and Nb_4C_3 MXenes in various biosensing applications.

Conclusion and future perspectives

In this review, we have investigated the development and implementation of 2D MXenes and their composites as signal transducer and a potential carrier of biomolecules for biosensing applications. MXene's superiority in biosensing as well as the challenging factors, are addressed in detail. Nb and Ti_2C-based MXenes in biosensing are reviewed thoroughly. Furthermore, Ti_3C_2 MXene-based Sandwich immunoassays which ought to be highlighted are also reviewed. MXenes serve as a supporting substrate for the *in situ* growth of nanoparticles, which offers an additional degree of freedom for tuning their biosensor's performance. Based on the above studies, it is evident that MXenes offer a fertile platform to develop efficient biosensors and can facilitate substantial innovations in biosensing research. In addition to MXene's inherent biocompatibility, their high mechanical strength and ease of post-processing have anticipated new perspectives for miniature devices and implantable prototypes. Due to their controllable surface chemistry, intrinsic conductivity, ease of functionalization, and the possibility of forming composites with metal nanoparticles, MXenes are superior to currently available 2D materials when it comes to sensing or biosensing applications. Despite this, there are some major challenges, such as the reproducibility of MXene sensors, and certain other limitations are associated with them. A safe, economical, and HF-free method should be developed to achieve thin 2D layers of MXene without following post-processing steps. Avoiding delamination is cost-effective, and on contrary, sonication results in surface defects that negatively affect MXene's properties. MXene's low oxidation stability severely hampers its long shelf life, therefore limiting its application in onsite clinical analysis. Multiple approaches are reported so far and summarized in the text above, specifically the inclusion of foreign species (*e.g.*, ionic salts for edge capping) may impede the charge transport among the sheets. Therefore, detailed charge transport studies, optimization of these protocols, and the development of new synthesis routes are needed to unlock the antioxidation abilities of MXenes. Functional groups confer important properties to the MXenes, such as semiconducting behaviour, and offer profuse loading of biorecognition elements, however, controlling their surface chemistry is still

challenging. Increasing chemical & temperature stability and synthesizing termination-free and/or uniformly terminated structures can help to realize their maximum potential. Bottom-up synthesis methods can provide a better control over the surface defects, tuning the active sites for molecular interactions, and controlled adsorption of analytes. The basic mechanism of how MXene surfaces interact with biological molecules is still unknown. Quantification and orientation of biomolecules on MXene's surface as well as monitoring the adsorption kinetics can determine their sensing performance. It is also important to use simple and efficient biofunctionalization techniques. For instance, Photochemical Immobilization Technique (PIT) can tether antibodies in an oriented way, and it requires the use of gold interacting surfaces, such as gold nanoparticles.[184] PIT ensures control on the orientation of Ab's, while AuNPs offer synergistic effects with MXene sheets. Such an approach in MXene-based electrochemical immunosensors can significantly enhance the sensitivity. It would also be intriguing to understand the direct interaction between Ab's and terminations on the MXene surface without mediators. It can allow control over MXene's surface chemistry and can be used to design novel structures. DTM MXenes have emerged just recently and have great potential with better properties than conventional mono-MXenes. The application of such MXenes can open new avenues and solve current problems in the field of MXene sensing. Patently, MXenes have made their way in biosensing and have been used extensively to enhance sensitivity. But it is required to standardize the characterization protocols and, the performance criteria of MXene-sensors must be outlined for industrial applications. Ti_3C_2 MXene is excessively employed in biosensors and has left a huge research gap with other MXenes structures such as V_2C, Nb_2C, and Nb_4C_3. As these structures exhibit exceptional features in biosensing, they should be utilized to fill this void in MXenes research and can help the commercialization of MXenes sensors. The ability to control the physical and chemical structure and, particularly as it relates to biosensors, understanding the fundamental interaction mechanisms of this new 2D system, can further strengthen the current knowledge of the field. Certainly, 2D MXenes have salient properties and have a place in the biosensing field, however, this requires cross-disciplinary efforts and cutting-edge research.

Conflicts of interest

There are no conflicts to declare.

References

1 K. Kalantar-Zadeh and J. Z. Ou, *ACS Sens.*, 2016, **1**, 5–16.
2 T. Kuila, S. Bose, P. Khanra, A. K. Mishra, N. H. Kim and J. H. Lee, *Biosens. Bioelectron.*, 2011, **26**, 4637–4648.
3 S. Liu and X. Guo, *NPG Asia Mater.*, 2012, **4**, e23.
4 M. Xu, T. Liang, M. Shi and H. Chen, *Chem. Rev.*, 2013, **113**, 3766–3798.
5 H. Zhang, *ACS Nano*, 2015, **9**, 9451–9469.
6 P. Martin, *Mater. Today*, 2011, **14**, 308–315.
7 L. Ou, B. Song, H. Liang, J. Liu, X. Feng, B. Deng, T. Sun and L. Shao, *Part. Fibre Toxicol.*, 2016, **13**(57), 1–24.
8 L. Liang, X. Peng, F. Sun, Z. Kong and J. W. Shen, *Nanoscale Adv.*, 2021, **3**, 904–917.
9 M. Coroș, S. Pruneanu and R.-I. Stefan-van Staden, *J. Electrochem. Soc.*, 2020, **167**, 037528.
10 C. Liao, Y. Li and S. C. Tjong, *Int. J. Mol. Sci.*, 2018, **19**, 3564.
11 M. Naguib, M. Kurtoglu, V. Presser, J. Lu, J. Niu, M. Heon, L. Hultman, Y. Gogotsi and M. W. Barsoum, *Adv. Mater.*, 2011, **23**, 4248–4253.
12 S. A. Zahra and S. Rizwan, *RSC Adv.*, 2022, **12**, 8405–8413.
13 X. Li, Z. Huang, C. E. Shuck, G. Liang, Y. Gogotsi and C. Zhi, *Nat. Rev. Chem.*, 2022, **6**, 389–404.
14 B. Anasori, M. R. Lukatskaya and Y. Gogotsi, *Nat. Rev. Mater.*, 2017, **2**, 16098.
15 M. Han, C. E. Shuck, R. Rakhmanov, D. Parchment, B. Anasori, C. M. Koo, G. Friedman and Y. Gogotsi, *ACS Nano*, 2020, **14**, 5008–5016.
16 A. Zamhuri, G. P. Lim, N. L. Ma, K. S. Tee and C. F. Soon, *Biomed. Eng. Online*, 2021, **20**, 1–24.
17 J. Liu, W. Peng, Y. Li, F. Zhang and X. Fan, *Trans. Tianjin Univ.*, 2020, **26**, 149–171.
18 Q. Li, Y. Li and W. Zeng, *Chemosensors*, 2021, **9**, 225.
19 Z. Guo, J. Zhou, L. Zhu and Z. Sun, *J. Mater. Chem. A*, 2016, **4**, 11446–11452.
20 Z. U. D. Babar, J. Fatheema, N. Arif, M. S. Anwar, S. Gul, M. Iqbal and S. Rizwan, *RSC Adv.*, 2020, **10**, 25669–25678.
21 K. Luo, X. H. Zha, Q. Huang, C. te Lin, M. Yang, S. Zhou and S. Du, *RSC Adv.*, 2020, **10**, 44430–44436.
22 Q. Noor, S. A. Zahra, M. I. Serna, C. K. Abuoudah, M. Z. Iqbal, D. Akinwande and S. Rizwan, *Ceram. Int.*, 2020, **46**, 27419–27425.
23 J. Bekaert, C. Sevik and M. v. Miloševic, *Nanoscale*, 2020, **12**, 17354–17361.
24 K. Wang, H. Jin, H. Li, Z. Mao, L. Tang, D. Huang, J. H. Liao and J. Zhang, *Surf. Interfaces*, 2022, **29**, 101711.
25 Z. U. D. Babar, M. S. Anwar, M. Mumtaz, M. Iqbal, R. K. Zheng, D. Akinwande and S. Rizwan, *2D Mater.*, 2020, **7**, 035012.
26 T. Ouisse and M. W. Barsoum, *Mater. Res. Lett.*, 2017, **5**, 365–378.
27 Z. U. D. Babar, R. K. Zheng, M. Mumtaz and S. Rizwan, *Mater. Lett.*, 2021, **285**, 129210.
28 Y. Gogotsi and B. Anasori, *ACS Nano*, 2019, **13**, 8491–8494.
29 D. Xu, Z. Li, L. Li and J. Wang, *Adv. Funct. Mater.*, 2020, **30**, 2000712.
30 M. Ghidiu, M. R. Lukatskaya, M. Q. Zhao, Y. Gogotsi and M. W. Barsoum, *Nature*, 2015, **516**, 78–81.
31 M. Mozafari and M. Soroush, *Mater. Adv.*, 2021, **2**, 7277–7307.
32 G. P. Lim, C. F. Soon, N. L. Ma, M. Morsin, N. Nayan, M. K. Ahmad and K. S. Tee, *Environ. Res.*, 2021, **201**, 111592.
33 H. Zhou, F. Wang, Y. Wang, C. Li, C. Shi, Y. Liu and Z. Ling, *RSC Adv.*, 2021, **11**, 5512–5520.
34 T. S. Mathis, K. Maleski, A. Goad, A. Sarycheva, M. Anayee, A. C. Foucher, K. Hantanasirisakul, C. E. Shuck, E. A. Stach and Y. Gogotsi, *ACS Nano*, 2021, **15**, 6420–6429.

35 Z. Liu and H. N. Alshareef, *Adv. Electron. Mater.*, 2021, **7**, 2100295.
36 F. G. Zamani, H. Moulahoum, M. Ak, D. O. Demirkol and S. Timur, *TrAC, Trends Anal. Chem.*, 2019, **118**, 264–276.
37 S. Ramanavicius and A. Ramanavicius, *Nanomaterials*, 2021, **11**, 1–22.
38 C. S. Park, C. Lee and O. S. Kwon, *Polymers*, 2016, **8**, 249.
39 K. Namsheer and C. S. Rout, *RSC Adv.*, 2021, **11**, 5659–5697.
40 M. O. Faruk, A. Ahmed, B. Adak, M. Marzana, M. M. Hossain and S. Mukhopadhyay, *J. Mater. Chem. C*, 2021, **9**, 10193–10215.
41 B. Yao, J. Yao, Z. Fan, J. Zhao, K. Zhang and W. Huang, *ChemElectroChem*, 2022, **9**, e202200103.
42 M. Mathew and C. S. Rout, *Curr. Opin. Electrochem.*, 2021, **30**, 100782.
43 A. Rhouati, M. Berkani, Y. Vasseghian and N. Golzadeh, *Chemosphere*, 2022, **291**(part 1), 132921.
44 S. K. Bhardwaj, H. Singh, M. Khatri, K. H. Kim and N. Bhardwaj, *Biosens. Bioelectron.*, 2022, **202**, 113995.
45 S. Ramanavicius and A. Ramanavicius, *Int. J. Mol. Sci.*, 2020, **21**, 1–17.
46 J. Gonzalez-Julian, *J. Am. Ceram. Soc.*, 2021, **104**, 659–690.
47 N. C. Frey, J. Wang, G. I. V. Bellido, B. Anasori, Y. Gogotsi and V. B. Shenoy, *ACS Nano*, 2019, **13**, 3031–3041.
48 J. Pan, S. Lany and Y. Qi, *ACS Nano*, 2017, **11**, 7560–7564.
49 R. Syamsai and A. N. Grace, *J. Alloys Compd.*, 2019, **792**, 1230–1238.
50 Q. Tao, M. Dahlqvist, J. Lu, S. Kota, R. Meshkian, J. Halim, J. Palisaitis, L. Hultman, M. W. Barsoum, P. O. Å. Persson and J. Rosen, *Nat. Commun.*, 2017, **8**, 14949.
51 M. Naguib, J. Halim, J. Lu, K. M. Cook, L. Hultman, Y. Gogotsi and M. W. Barsoum, *J. Am. Chem. Soc.*, 2013, **135**, 15966–15969.
52 M. Ghidiu, M. Naguib, C. Shi, O. Mashtalir, L. M. Pan, B. Zhang, J. Yang, Y. Gogotsi, S. J. L. Billinge and M. W. Barsoum, *Chem. Commun.*, 2014, **50**, 9517–9520.
53 C. E. Shuck, A. Sarycheva, M. Anayee, A. Levitt, Y. Zhu, S. Uzun, V. Balitskiy, V. Zahorodna, O. Gogotsi and Y. Gogotsi, *Adv. Eng. Mater.*, 2020, **22**, 1901241.
54 C. E. Shuck, K. Ventura-Martinez, A. Goad, S. Uzun, M. Shekhirev and Y. Gogotsi, *ACS Chem. Health Saf.*, 2021, **28**, 326–338.
55 M. Alhabeb, K. Maleski, B. Anasori, P. Lelyukh, L. Clark, S. Sin and Y. Gogotsi, *Chem. Mater.*, 2017, **29**, 7633–7644.
56 A. S. Levitt, M. Alhabeb, C. B. Hatter, A. Sarycheva, G. Dion and Y. Gogotsi, *J. Mater. Chem. A*, 2019, **7**, 269–277.
57 N. Driscoll, A. G. Richardson, K. Maleski, B. Anasori, O. Adewole, P. Lelyukh, L. Escobedo, D. K. Cullen, T. H. Lucas, Y. Gogotsi and F. Vitale, *ACS Nano*, 2018, **12**, 10419–10429.
58 A. Lipatov, M. Alhabeb, M. R. Lukatskaya, A. Boson, Y. Gogotsi and A. Sinitskii, *Adv. Electron. Mater.*, 2016, **2**, 1600255.
59 A. Iqbal, P. Sambyal, J. Kwon, M. Han, J. Hong, S. J. Kim, M. K. Kim, Y. Gogotsi and C. M. Koo, *Compos. Sci. Technol.*, 2021, **213**, 108878.
60 V. Natu, R. Pai, M. Sokol, M. Carey, V. Kalra and M. W. Barsoum, *Chem*, 2020, **6**, 616–630.
61 T. Li, L. Yao, Q. Liu, J. Gu, R. Luo, J. Li, X. Yan, W. Wang, P. Liu, B. Chen, W. Zhang, W. Abbas, R. Naz and D. Zhang, *Angew. Chem.*, 2018, **130**, 6223–6227.
62 L. Li, G. Li, L. Tan, Y. Zhang and B. Wu, *Langmuir*, 2017, **33**, 9000–9006.
63 S. Yang, P. Zhang, F. Wang, A. G. Ricciardulli, M. R. Lohe, P. W. M. Blom and X. Feng, *Angew. Chem., Int. Ed.*, 2018, **57**, 15491–15495.
64 H. Shi, P. Zhang, Z. Liu, S. W. Park, M. R. Lohe, Y. Wu, A. S. Nia, S. Yang and X. Feng, *Angew. Chem., Int. Ed.*, 2021, **60**, 8689–8693.
65 R. A. Vaia, A. Jawaid, A. Hassan, G. Neher, D. Nepal, R. Pachter, W. J. Kennedy and S. Ramakrishnan, *ACS Nano*, 2021, **15**, 2771–2777.
66 K. Arole, J. W. Blivin, S. Saha, D. E. Holta, X. Zhao, A. Sarmah, H. Cao, M. Radovic, J. L. Lutkenhaus and M. J. Green, *iScience*, 2021, **24**, 103403.
67 H. Dong, P. Xiao, N. Jin, B. Wang, Y. Liu and Z. Lin, *ChemElectroChem*, 2021, **8**, 957–962.
68 L. Liu, M. Orbay, S. Luo, S. Duluard, H. Shao, J. Harmel, P. Rozier, P. L. Taberna and P. Simon, *ACS Nano*, 2022, **16**, 111–118.
69 M. Sokol, V. Natu, S. Kota and M. W. Barsoum, *Trends Chem.*, 2019, **1**, 210–223.
70 Y. Gogotsi, *Nanomaterials Handbook*, CRC Press, 2nd edn, 2017.
71 K. Maleski, C. E. Ren, M. Q. Zhao, B. Anasori and Y. Gogotsi, *ACS Appl. Mater. Interfaces*, 2018, **10**, 24491–24498.
72 M. Naguib, R. R. Unocic, B. L. Armstrong and J. Nanda, *Dalton Trans.*, 2015, **44**, 9353.
73 M. Naguib, V. N. Mochalin, M. W. Barsoum and Y. Gogotsi, *Adv. Mater.*, 2014, **26**, 992–1005.
74 K. J. Harris, M. Bugnet, M. Naguib, M. W. Barsoum and G. R. Goward, *J. Phys. Chem. C*, 2015, **119**, 13713–13720.
75 I. Persson, L. Å. Näslund, J. Halim, M. W. Barsoum, V. Darakchieva, J. Palisaitis, J. Rosen and P. O. Å. Persson, *2D Mater.*, 2018, **5**, 015002.
76 H. W. Wang, M. Naguib, K. Page, D. J. Wesolowski and Y. Gogotsi, *Chem. Mater.*, 2016, **28**, 349–359.
77 X. Wang, X. Shen, Y. Gao, Z. Wang, R. Yu and L. Chen, *J. Am. Chem. Soc.*, 2015, **137**, 2715–2721.
78 M. Seredych, C. E. Shuck, D. Pinto, M. Alhabeb, E. Precetti, G. Deysher, B. Anasori, N. Kurra and Y. Gogotsi, *Chem. Mater.*, 2019, **31**, 3324–3332.
79 M. A. Hope, A. C. Forse, K. J. Griffith, M. R. Lukatskaya, M. Ghidiu, Y. Gogotsi and C. P. Grey, *Phys. Chem. Chem. Phys.*, 2016, **18**, 5099–5102.
80 I. Persson, J. Halim, T. W. Hansen, J. B. Wagner, V. Darakchieva, J. Palisaitis, J. Rosen and P. O. Å. Persson, *Adv. Funct. Mater.*, 2020, **30**, 1909005.
81 J. L. Hart, K. Hantanasirisakul, A. C. Lang, B. Anasori, D. Pinto, Y. Pivak, J. T. van Omme, S. J. May, Y. Gogotsi and M. L. Taheri, *Nat. Commun.*, 2019, **10**, 522.
82 O. Mashtalir, M. Naguib, V. N. Mochalin, Y. Dall'Agnese, M. Heon, M. W. Barsoum and Y. Gogotsi, *Nat. Commun.*, 2013, **4**, 1716.

83 A. VahidMohammadi, J. Rosen and Y. Gogotsi, *Science*, 2021, **372**, 6547.
84 M. Shekhirev, C. E. Shuck, A. Sarycheva and Y. Gogotsi, *Prog. Mater. Sci.*, 2021, **120**, 100757.
85 M. Naguib, O. Mashtalir, J. Carle, V. Presser, J. Lu, L. Hultman, Y. Gogotsi and M. W. Barsoum, *ACS Nano*, 2012, **6**, 1322–1331.
86 E. Satheeshkumar, T. Makaryan, A. Melikyan, H. Minassian, Y. Gogotsi and M. Yoshimura, *Sci. Rep.*, 2016, **6**, 32049.
87 K. Maleski, V. N. Mochalin and Y. Gogotsi, *Chem. Mater.*, 2017, **29**, 1632–1640.
88 C. Wang, S. Chen and L. Song, *Adv. Funct. Mater.*, 2020, **30**, 2000869.
89 L. Gao, W. Bao, A. v. Kuklin, S. Mei, H. Zhang and H. Ågren, *Adv. Mater.*, 2021, **33**, 2004129.
90 J. Zou, J. Wu, Y. Wang, F. Deng, J. Jiang, Y. Zhang, S. Liu, N. Li, H. Zhang, J. Yu, T. Zhai and H. N. Alshareef, *Chem. Soc. Rev.*, 2022, **51**, 2972–2990.
91 J. Wu, Y. Yu and G. Su, *Nanomaterials*, 2022, **12**, 828.
92 H. Shao, K. Xu, Y. C. Wu, A. Iadecola, L. Liu, H. Ma, L. Qu, E. Raymundo-Piñero, J. Zhu, Z. Lin, P. L. Taberna and P. Simon, *ACS Energy Lett.*, 2020, **5**, 2873–2880.
93 H. Dong, L. Cao, Z. Tan, Q. Liu, J. Zhou, P. Zhao, P. Wang, Y. Li, W. Ma and Y. Dong, *ACS Appl. Bio Mater.*, 2020, **3**, 377–384.
94 B. Xu, M. Zhu, W. Zhang, X. Zhen, Z. Pei, Q. Xue, C. Zhi and P. Shi, *Adv. Mater.*, 2016, **28**, 3333–3339.
95 F. Liu, Y. Liu, X. Zhao, K. Liu, H. Yin and L. Z. Fan, *Small*, 2022, **16**, 1906076.
96 B. Xu, C. Zhi and P. Shi, *JPhys Mater.*, 2020, **3**, 031001.
97 D. Wen, X. Wang, L. Liu, C. Hu, C. Sun, Y. Wu, Y. Zhao, J. Zhang, X. Liu and G. Ying, *ACS Appl. Mater. Interfaces*, 2021, **13**, 17766–17780.
98 K. Hantanasirisakul, M. Q. Zhao, P. Urbankowski, J. Halim, B. Anasori, S. Kota, C. E. Ren, M. W. Barsoum and Y. Gogotsi, *Adv. Electron. Mater.*, 2016, **2**, 1600050.
99 W. Hong, B. C. Wyatt, S. K. Nemani and B. Anasori, *MRS Bull.*, 2020, **45**, 850–861.
100 I. Persson, A. el Ghazaly, Q. Tao, J. Halim, S. Kota, V. Darakchieva, J. Palisaitis, M. W. Barsoum, J. Rosen and P. O. Å. Persson, *Small*, 2018, **14**, 1703676.
101 C. J. Zhang, S. Pinilla, N. McEvoy, C. P. Cullen, B. Anasori, E. Long, S. H. Park, A. Seral-Ascaso, A. Shmeliov, D. Krishnan, C. Morant, X. Liu, G. S. Duesberg, Y. Gogotsi and V. Nicolosi, *Chem. Mater.*, 2017, **29**, 4848–4856.
102 X. Zhao, A. Vashisth, E. Prehn, W. Sun, S. A. Shah, T. Habib, Y. Chen, Z. Tan, J. L. Lutkenhaus, M. Radovic and M. J. Green, *Matter*, 2019, **1**, 513–526.
103 S. Huang and V. N. Mochalin, *Inorg. Chem.*, 2019, **58**, 1958–1966.
104 V. Natu, J. L. Hart, M. Sokol, H. Chiang, M. L. Taheri and M. W. Barsoum, *Angew. Chem.*, 2019, **131**, 12785–12790.
105 E. Choi, J. Lee, Y. J. Kim, H. Kim, M. Kim, J. Hong, Y. C. Kang, C. M. Koo, D. W. Kim and S. J. Kim, *Carbon*, 2022, **191**, 593–599.
106 R. Ibragimova, P. Rinke and H. P. Komsa, *Chem. Mater.*, 2022, **34**, 2896–2906.
107 F. Xia, J. Lao, R. Yu, X. Sang, J. Luo, Y. Li and J. Wu, *Nanoscale*, 2019, **11**, 23330–23337.
108 V. Natu, M. Sokol, L. Verger and M. W. Barsoum, *J. Phys. Chem. C*, 2018, **122**, 27745–27753.
109 R. Lotfi, M. Naguib, D. E. Yilmaz, J. Nanda and A. C. T. van Duin, *J. Mater. Chem. A*, 2018, **6**, 12733–12743.
110 H. Ghassemi, W. Harlow, O. Mashtalir, M. Beidaghi, M. R. Lukatskaya, Y. Gogotsi and M. L. Taheri, *J. Mater. Chem. A*, 2014, **2**, 14339–14343.
111 E. Lira, S. Wendt, P. Huo, J. Hansen, R. Streber, S. Porsgaard, Y. Wei, R. Bechstein, E. Lægsgaard and F. Besenbacher, *J. Am. Chem. Soc.*, 2011, **133**, 6529–6532.
112 Y. Chae, S. J. Kim, S. Y. Cho, J. Choi, K. Maleski, B. J. Lee, H. T. Jung, Y. Gogotsi, Y. Lee and C. W. Ahn, *Nanoscale*, 2019, **11**, 8387–8393.
113 S. Ramanavicius and A. Ramanavicius, *Sensors*, 2020, **20**, 1–18.
114 S. Ramanavicius, A. Jagminas and A. Ramanavicius, *Coatings*, 2022, **12**, 699.
115 F. Wang, C. H. Yang, M. Duan, Y. Tang and J. F. Zhu, *Biosens. Bioelectron.*, 2015, **74**, 1022–1028.
116 L. Lorencova, T. Bertok, J. Filip, M. Jerigova, D. Velic, P. Kasak, K. A. Mahmoud and J. Tkac, *Sens. Actuators, B*, 2018, **263**, 360–368.
117 P. A. Rasheed, R. P. Pandey, K. A. Jabbar, J. Ponraj and K. A. Mahmoud, *Anal. Methods*, 2019, **11**, 3851–3856.
118 H. Lin, S. Gao, C. Dai, Y. Chen and J. Shi, *J. Am. Chem. Soc.*, 2017, **139**, 16235–16247.
119 Z. Huang, X. Cui, S. Li, J. Wei, P. Li, Y. Wang and C. S. Lee, *Nanophotonics*, 2020, **9**, 2233–2249.
120 J. Xuan, Z. Wang, Y. Chen, D. Liang, L. Cheng, X. Yang, Z. Liu, R. Ma, T. Sasaki and F. Geng, *Angew. Chem.*, 2016, **128**, 14789–14794.
121 P. K. Kalambate, N. S. Gadhari, X. Li, Z. Rao, S. T. Navale, Y. Shen, V. R. Patil and Y. Huang, *TrAC, Trends Anal. Chem.*, 2019, **120**, 115643.
122 K. Li, T. Jiao, R. Xing, G. Zou, J. Zhou, L. Zhang and Q. Peng, *Sci. China Mater.*, 2018, **61**, 728–736.
123 H. Zou, F. Zhang, H. Wang, J. Xia, L. Gao and Z. Wang, *New J. Chem.*, 2019, **43**, 2464–2470.
124 R. B. Rakhi, P. Nayuk, C. Xia and H. N. Alshareef, *Sci. Rep.*, 2016, **6**, 36422.
125 S. Elumalai, V. Mani, N. Jeromiyas, V. K. Ponnusamy and M. Yoshimura, *Microchim. Acta*, 2020, **187**, 33.
126 Y. Wang, S. Liu, F. Zhu, Y. Gan and Q. Wen, *Nanomaterials*, 2021, **11**, 1995.
127 M. Seredych, K. Maleski, T. S. Mathis and Y. Gogotsi, *Colloids Surf., A*, 2022, **641**, 128580.
128 L. Zhou, X. Zhang, L. Ma, J. Gao and Y. Jiang, *Biochem. Eng. J.*, 2017, **128**, 243–249.
129 Y. Jiang, X. Zhang, L. Pei, S. Yue, L. Ma, L. Zhou, Z. Huang, Y. He and J. Gao, *Chem. Eng. J.*, 2018, **339**, 547–556.
130 D. Song, X. Jiang, Y. Li, X. Lu, S. Luan, Y. Wang, Y. Li and F. Gao, *J. Hazard. Mater.*, 2019, **373**, 367–376.
131 H. Zhang, Z. Wang, Q. Zhang, F. Wang and Y. Liu, *Biosens. Bioelectron.*, 2019, **124–125**, 184–190.

132 Y. Wang, Z. Zeng, J. Qiao, S. Dong, Q. Liang and S. Shao, *Talanta*, 2021, **221**, 121605.
133 R. Stephanie, M. W. Kim, S. H. Kim, J. K. Kim, C. Y. Park and T. J. Park, *TrAC, Trends Anal. Chem.*, 2021, **135**, 116159.
134 F. Zhao, Y. Yao, C. Jiang, Y. Shao, D. Barceló, Y. Ying and J. Ping, *J. Hazard. Mater.*, 2020, **384**, 121358.
135 J. Zheng, B. Wang, A. Ding, B. Weng and J. Chen, *J. Electroanal. Chem.*, 2018, **816**, 189–194.
136 F. Shahzad, A. Iqbal, S. A. Zaidi, S. W. Hwang and C. M. Koo, *J. Ind. Eng. Chem.*, 2019, **79**, 338–344.
137 M. Mohammadniaei, A. Koyappayil, Y. Sun, J. Min and M. H. Lee, *Biosens. Bioelectron.*, 2020, **159**, 112208.
138 S. Adomavičiūtė-Grabusovė, S. Ramanavičius, A. Popov, V. Šablinskas, O. Gogotsi and A. Ramanavičius, *Chemosensors*, 2021, **9**, 223.
139 Y. Peng, C. Lin, L. Long, T. Masaki, M. Tang, L. Yang, J. Liu, Z. Huang, Z. Li, X. Luo, J. R. Lombardi and Y. Yang, *Nano-Micro Lett.*, 2021, **13**, 52.
140 K. Shevchuk, A. Sarycheva and Y. Gogotsi, *MRS Bull.*, 2022, **47**, DOI: 10.1557/s43577-022-00276-8.
141 Y. Zhao, X. Yang, H. Li, Y. Luo, R. Yu, L. Zhang, Y. Yang and Q. Song, *Chem. Commun.*, 2015, **51**, 16908–16911.
142 S. Cong, Y. Yuan, Z. Chen, J. Hou, M. Yang, Y. Su, Y. Zhang, L. Li, Q. Li, F. Geng and Z. Zhao, *Nat. Commun.*, 2015, **6**, 7800.
143 F. Zheng, W. Ke, L. Shi, H. Liu and Y. Zhao, *Anal. Chem.*, 2019, **91**, 11812–11820.
144 H. Medetalibeyoglu, G. Kotan, N. Atar and M. L. Yola, *Anal. Chim. Acta*, 2020, **1139**, 100–110.
145 K. S. Novoselov, A. Mishchenko, A. Carvalho and A. H. C. Neto, *Science*, 2016, **353**(6298), aac9439.
146 N. Martín, N. Tagmatarchis, Q. H. Wang and X. Zhang, *Chem.–Eur. J.*, 2020, **26**, 6292–6295.
147 J. Song, M. Li, H. Liang and H. Lou, *Comput. Theor. Chem.*, 2017, **1118**, 115–122.
148 J. D. Gouveia, G. Novell-Leruth, F. Viñes, F. Illas and J. R. B. Gomes, *Appl. Surf. Sci.*, 2021, **544**, 148946.
149 J. D. Gouveia, G. Novell-Leruth, P. M. L. S. Reis, F. Viñes, F. Illas and J. R. B. Gomes, *ACS Appl. Bio Mater.*, 2020, **3**, 5913–5921.
150 A. Vaidyanathan, M. Mathew, S. Radhakrishnan, C. S. Rout and B. Chakraborty, *J. Phys. Chem. B*, 2020, **124**, 11098–11122.
151 V. Chaudhary, A. Kaushik, H. Furukawa and A. Khosla, *ECS Sensors Plus*, 2022, **1**, 013601.
152 R. Li, L. Zhang, L. Shi and P. Wang, *ACS Nano*, 2017, **11**, 3752–3759.
153 C. L. Manzanares-Palenzuela, A. M. Pourrahimi, J. Gonzalez-Julian, Z. Sofer, M. Pykal, M. Otyepka and M. Pumera, *Chem. Sci.*, 2019, **10**, 10010–10017.
154 X. Wu, P. Ma, Y. Sun, F. Du, D. Song and G. Xu, *Electroanalysis*, 2021, **33**, 1827–1851.
155 X. Li, Y. Lu and Q. Liu, *Talanta*, 2021, **235**, 122726.
156 R. Thenmozhi, S. Maruthasalamoorthy, R. Nirmala and R. Navamathavan, *J. Electrochem. Soc.*, 2021, **168**, 117507.
157 F. Shahzad, S. A. Zaidi and R. A. Naqvi, *Crit. Rev. Anal. Chem.*, 2020, **52**, 848–864.
158 S. Kumar, Y. Lei, N. H. Alshareef, M. A. Quevedo-Lopez and K. N. Salama, *Biosens. Bioelectron.*, 2018, **121**, 243–249.
159 T. Su, X. Ma, J. Tong, H. Ji, Z. Qin and Z. Wu, *J. Mater. Chem. A*, 2022, **10**, 10265–10296.
160 M. Mozafari and M. Soroush, *Mater. Adv.*, 2021, **2**, 7277–7307.
161 H. Medetalibeyoglu, M. Beytur, O. Akyıldırım, N. Atar and M. L. Yola, *Sens. Actuators, B*, 2020, **319**, 128195.
162 H. Medetalibeyoglu, G. Kotan, N. Atar and M. L. Yola, *Talanta*, 2020, **220**, 121403.
163 S. Su, Q. Sun, X. Gu, Y. Xu, J. Shen, D. Zhu, J. Chao, C. Fan and L. Wang, *TrAC, Trends Anal. Chem.*, 2019, **119**, 115610.
164 Y. Xu, Y. S. Ang, L. Wu and L. K. Ang, *Nanomaterials*, 2019, **9**, 165.
165 L. Wu, Q. You, Y. Shan, S. Gan, Y. Zhao, X. Dai and Y. Xiang, *Sens. Actuators, B*, 2018, **277**, 210–215.
166 Q. Wu, N. Li, Y. Wang, Y. liu, Y. Xu, S. Wei, J. Wu, G. Jia, X. Fang, F. Chen and X. Cui, *Biosens. Bioelectron.*, 2019, **144**, 111697.
167 Q. Wu, N. Li, Y. Wang, Y. Xu, J. Wu, G. Jia, F. Ji, X. Fang, F. Chen and X. Cui, *Anal. Chem.*, 2020, **92**, 3354–3360.
168 J. Feng, Y. Xu, W. Huang, H. Kong, Y. Li, H. Cheng and L. Li, *Anal. Chim. Acta*, 2020, **1097**, 176–185.
169 J. Cheng, K. Hu, Q. Liu, Y. Liu, H. Yang and J. Kong, *Anal. Bioanal. Chem.*, 2021, **413**, 2543–2551.
170 K. Hu, J. Cheng, K. Wang, Y. Zhao, Y. Liu, H. Yang and Z. Zhang, *Talanta*, 2022, **238**(part 1), 122987.
171 H. Zhang, Z. Wang, Q. Zhang, F. Wang and Y. Liu, *Biosens. Bioelectron.*, 2019, **124–125**, 184–190.
172 H. Zhang, Z. Wang, F. Wang, Y. Zhang, H. Wang and Y. Liu, *Anal. Chem.*, 2020, **92**, 5553.
173 L. Shang, X. Wang, W. Zhang, L. P. Jia, R. N. Ma, W. L. Jia and H. S. Wang, *Sens. Actuators, B*, 2020, **325**, 128776.
174 X. Zhu, P. Liu, T. Xue, Y. Ge, S. Ai, Y. Sheng, R. Wu, L. Xu, K. Tang and Y. Wen, *Ceram. Int.*, 2021, **47**, 173–184.
175 S. Gan, B. Ruan, Y. Xiang and X. Dai, *IEEE Sens. J.*, 2021, **21**, 347–352.
176 J. Yin, S. Pan, X. Guo, Y. Gao, D. Zhu, Q. Yang, J. Gao, C. Zhang and Y. Chen, *Nano-Micro Lett.*, 2021, **13**, 30.
177 N. Arif, S. Gul, M. Sohail, S. Rizwan and M. Iqbal, *Ceram. Int.*, 2021, **47**, 2388–2396.
178 M. Lian, Y. Shi, W. Zhang, J. Zhao and D. Chen, *J. Electroanal. Chem.*, 2021, **904**, 115849.
179 P. A. Rasheed, R. P. Pandey, T. Gomez, K. A. Jabbar, K. Prenger, M. Naguib, B. Aïssa and K. A. Mahmoud, *Electrochem. Commun.*, 2020, **119**, 106811.
180 P. A. Rasheed, R. P. Pandey, T. Gomez, M. Naguib and K. A. Mahmoud, *RSC Adv.*, 2020, **10**, 24697–24704.
181 P. A. Rasheed, R. P. Pandey, K. A. Jabbar and K. A. Mahmoud, *Electroanalysis*, 2022, **34**, 1–8.
182 D. Fang, H. Ren, Y. Huang, H. Dai, D. Huang and Y. Lin, *Sens. Actuators, B*, 2020, **312**, 127950.
183 M. Song, S. Y. Pang, F. Guo, M. C. Wong and J. Hao, *Adv. Sci.*, 2020, **7**, 2001546.
184 B. della Ventura, M. Banchelli, R. Funari, A. Illiano, M. de Angelis, P. Taroni, A. Amoresano, P. Matteini and R. Velotta, *Analyst*, 2019, **144**, 6871–6880.